J. Fluid Mech. (1996), vol. 313, pp. 241–282

Non-Gaussian scalar statistics in homogeneous turbulence

By F. A. JABERI, R. S. MILLER, C. K. MADNIA AND P. GIVI

Department of Mechanical and Aerospace Engineering, State University of New York at Buffalo, Buffalo, NY 14260-4400, USA

(Received 1 November 1994 and in revised form 18 September 1995)

Results are presented of numerical simulations of passive scalar mixing in homogeneous, incompressible turbulent flows. These results are generated via the Linear Eddy Model (LEM) and Direct Numerical Simulation (DNS) of turbulent flows under a variety of different conditions. The nature of mixing and its response to the turbulence field is examined and the single-point probability density function (p.d.f.) of the scalar amplitude and the p.d.f.s of the scalar spatial-derivatives are constructed. It is shown that both Gaussian and exponential scalar p.d.f.s emerge depending on the parameters of the simulations and the initial conditions of the scalar field. Aided by the analyses of data, several reasons are identified for the non-Gaussian behaviour of the scalar amplitude. In particular, two mechanisms are identified for causing exponential p.d.f.s: (i) a non-uniform action of advection on the large and the small scalar scales, (ii) the nonlinear interaction of the scalar and the velocity fluctuations at small scales. In the absence of a constant non-zero mean scalar gradient, the behaviour of the scalar p.d.f. is very sensitive to the initial conditions. In the presence of this gradient, an exponential p.d.f. is not sustained regardless of initial conditions. The numerical results pertaining to the small-scale intermittency (non-Gaussian scalar derivatives) are in accord with laboratory experimental results. The statistics of the scalar derivatives and those of the velocity-scalar fluctuations are also in accord with laboratory measured results.

1. Introduction

It has been more than four decades since Hawthorne, Weddell & Hottel (1949) indicated the advantages of the probability density function (p.d.f.) method for statistical description of reacting turbulent flows. Since then, p.d.f. methods have been used rather extensively as witnessed by many review articles devoted to the topic (Toor 1975; Pope 1979; Libby & Williams 1980, 1994; O'Brien 1980; Pope 1985, 1990); for the latest review, see Dopazo (1994). The systematic means of determining the p.d.f. involves the solution of the transport equation governing its evolution. In this equation, however, the effects of molecular action do not appear in a closed form and can be described only by means of employing an external model. In many of the previous applications, this problem has been overcome through the use of the Coalescence/Dispersion (C/D) models. Examples are the early C/D prototype of Curl (1963), the Linear Mean Square Estimation (LMSE) theory of Dopazo & O'Brien (1976), and the closure of Janicka, Kolbe & Kollmann (1979) amongst others. While not all of these closures were originally presented in a C/D form, it is now

established that the majority of those in current use (including the three mentioned above) can be cast in a generalized C/D mould (Pope 1982; McMurtry & Givi 1989).

None of the C/D closures currently in use are regarded as physically plausible – the primary reason being that they are not capable of producing an asymptotic 'Gaussian' p.d.f. for a scalar field in homogeneous turbulent flows. Such a Gaussian asymptotic state has been observed in several laboratory (Miyawaki, Tsujikawa & Uraguchi 1974; Tavoularis & Corrsin 1981*a*) and direct numerical simulation (DNS) (Givi & McMurtry 1988; Eswaran & Pope 1988; McMurtry & Givi 1989) results; see Givi (1989) for a review. This 'incapability' of the C/D models has been a driving force for the development of other mixing closures capable of generating Gaussian statistics. Examples are the age-biasing scheme of Pope (1982), the Amplitude Mapping Closure (AMC) of Kraichnan (1989) and Chen, Chen & Kraichnan (1989) and the Johnson-Edgeworth Translation (JET) of Miller *et al.* (1993). These models exhibit one common feature: They all yield an approximate asymptotic Gaussian scalar p.d.f. in homogeneous turbulent flows.

The results of some of the more recent laboratory and numerical experiments, however, indicate the possibility of distributions other than Gaussian. The measurements of Heslot, Castaing & Libchaber (1987), Castaing *et al.* (1989) and Sano, Wu & Libchaber (1989) (known as the Chicago group) show that the temperature fluctuations in the convective core of a Rayleigh–Bérnard cell are Gaussian when the Rayleigh number (Ra) is less than a critical value, but become 'exponential' when the magnitude of Ra exceeds the critical value. The results of numerical simulations (Christie & Domaradzki 1993, 1994) and laboratory experiments (Solomon and Gollub 1991) suggest that in addition to the Rayleigh number, the geometry of the cell and the magnitude of the Prandtl number also affect the statistics. Solomon (1990) shows that the temperature p.d.f. can be either Gaussian, exponential or a combination of the two throughout the convected core. Thoroddsen & Van Atta (1992) show that while the scalar derivative exhibits a strong exponential feature in stably stratified flows, the temperature fluctuations are governed by Gaussian statistics. The experiments of Jayesh & Warhaft (1991, 1992) reveal several characteristics of the p.d.f. of a passive temperature field in decaying homogeneous grid turbulence. For turbulent Reynolds numbers (based on the integral scale) $Re_l > 70$ they show that in the presence of a constant (non-zero) mean scalar gradient, the temperature p.d.f. is exponential, while for $Re_l < 70$ an approximate Gaussian p.d.f. is formed. These results are not in accord with those of earlier measurements of Tavoularis & Corrsin (1981*a*) who report a Gaussian scalar p.d.f. in the presence of a linear mean scalar profile in homogeneous shear flows for Reynolds numbers greater than 70. In the absence of the mean scalar gradient, Jayesh & Warhaft (1992) report a nearly Gaussian temperature p.d.f. regardless of the magnitude of the Reynolds number. Exponential scalar p.d.f.s are also reported in the experiments of Gollub *et al.* (1991) and Lane *et al.* (1993) conducted in a stirred flow with a constant mean scalar gradient and a near Gaussian velocity field. It is indicated, however, that by increasing the correlation length scale of the velocity field, the scalar statistics become Gaussian even at very large Reynolds numbers.

These recent experimental findings have motivated several analytical and computational investigations for the purpose of understanding the reasons for non-Gaussian scalar statistics. In an effort to explain the Chicago experiments, Yakhot (1989) modified an existing theory of passive scalar p.d.f.s (Sinai & Yakhot 1989) for the problem of Rayleigh–Bérnard convection. This formulation is based on the argument that the large-scale coherent vortex structures influence the hydrodynamic stability of the

thermal boundary layer, thus modifying the mechanism of turbulence production. Kimura & Kraichnan (1993) show that a nonlinear mean scalar profile and/or an 'active' scalar field can cause non-Gaussian statistics. The generated results for cases with a nonlinear mean scalar profile exhibit trends qualitatively similar to those in the Boussinesq convection experiments (Belmonte, Tilgner & Libchaber 1994; Siggia 1994). Pumir, Shraiman & Siggia (1991) and Holzer & Pumir (1993) propose a one-dimensional 'mean-field' phenomenological model based on which they argue that in the presence of a constant mean scalar gradient, non-Gaussian statistics emerge as an inherent property of random advection. Kerstein & McMurtry (1994*b*) argue that the exponential tails deduced from the mean-field theory are primarily due to the functional form of the advection process which is enacted by an 'additivity' assumption. They show that depending on the statistics of the advection field, a wide variety of scalar p.d.f.s (including Gaussian) can be generated. Using a two-dimensional model in which the velocity evolves under the Euler equation in a restricted band of wavenumbers, Holzer & Siggia (1994) show that exponential-like scalar p.d.f.s occur when the magnitude of the scalar dissipation is non-zero. Ching & Tu (1994) report results of two-dimensional simulations of a passive scalar advected by a solenoidal velocity field. Depending on the parameterization of the problem, the scalar p.d.f. may become non-Gaussian, even without the presence of the mean scalar gradient. Similar p.d.f.s are also observed in the large-eddy simulation results of Metais & Lesieur (1992). These observations indicate the need for more improved models for prediction of the scalar p.d.f. under different mixing scenarios (Jaberi & Givi 1995).

The phenomenon of small-scale 'intermittency', portrayed by non-Gaussian statistics of the derivative-field, has been the subject of widespread investigations in turbulence research since the original theory of Kolmogorov (1941). Although this theory remains the basis of nearly all turbulence research, it is an incomplete description of realistic turbulent flow in that it does not describe intermittency effects (Landau & Lifshitz 1959; Obukhov 1962; Kolmogorov 1962; Gurvich & Yaglom 1967; Monin & Yaglom 1975). Early experiments reveal that although the p.d.f. of the velocity field is Gaussian, the p.d.f. of velocity derivatives exhibit larger than Gaussian tails with departures increasing with the Reynolds number (Batchelor & Townsend 1949; Monin & Yaglom 1975; Yamamoto & Kambe 1991). These intermittent p.d.f.s are observed even for very low Reynolds number flows (Chen *et al.* 1993) and may occur in both the dissipation range and/or the inertial range of turbulence. The former is associated with non-Gaussian velocity derivatives. The latter is identified through the statistics of the two-point velocity difference (structure function) for inertial range separations and yields corrections to the $-5/3$ Kolmogorov energy spectrum scaling (Van Atta & Antonia 1980; Anselmet *et al.* 1984; Castaing, Gague & Hopfinger 1990; Vincent & Meneguzzi 1991).

The results of recent DNS experiments suggest that the regions of strongest vorticity are organized in elongated thin tubes, with thickness and length on the order of the Kolmogorov scale and the integral scale, respectively (Kerr 1985; Hosokawa & Yamamoto 1989; Vincent & Meneguzzi 1991; Tanaka & Kida 1993). Jimenez *et al.* (1993) observe that these tubes are a natural feature of turbulence, and do not depend on the particular forcing scheme employed. She (1990) and She & Orszag (1991) develop a 'two-fluid' model of intermittency which incorporates the existence of these organized structures. This model is capable of capturing the statistical behaviour of both the inertial- and the dissipation-range intermittency (She, Jackson & Orszag 1991). Most investigations of turbulent scalar mixing are for flows with Schmidt numbers of order unity ($Sc \sim 1$) for which the scalar spectral regimes

are analogous to those of the velocity field†. In this case, the application of the Kolmogorov (1941) description to the scalar is also inadequate due to an inability to account for intermittency. In particular, while the scalar fluctuations typically portray Gaussian statistics (Antonia & Van Atta 1978; Givi & McMurtry 1988; Eswaran & Pope 1988; McMurtry & Givi 1989), scalar derivatives and differences are known to exhibit larger tails with stronger departures than observed in the velocity statistics (Van Atta & Chen 1970; Antonia *et al.* 1984; Castaing *et al.* 1990; Miller *et al.* 1995). As with the hydrodynamics, the scalar field is known to be dominated by organized structures characterized by regions of strong scalar-derivative magnitude. Ruetsch & Maxey (1991 & 1992) show that regions of large scalar gradients form 'sheet-like' structures which are found to occur in regions of persistent straining of the flow field. It has also been shown (Kerr 1985; Ashurst, Chen & Rogers 1987*a*; Ashurst *et al.* 1987*b*; Nomura & Elghobashi 1992; Miller 1995) that the scalar gradient vector tends to align parallel to both the pressure gradient and the most compressive eigenvector of the strain-rate tensor in these regions. Miller *et al.* (1995) extend the two-fluid description of She (1990) to account for the role of scalar sheets in the dissipation-range scalar intermittency. While the results obtained in this way portray some features of small-scale scalar intermittency, the phenomenon of the non-Gaussian scalar-amplitude p.d.f. remains an unresolved issue.

1.1. *Objective*

The objective of this work is to demonstrate that there are several factors which determine the outcome of scalar mixing in homogeneous turbulent flows. The message to be conveyed is to confirm that the p.d.f. of the scalar can adopt many different forms and that the Gaussian form as indicated by Givi & McMurtry (1988), Eswaran & Pope (1988) and McMurtry & Givi (1989) is only one of the many possible outcomes. In doing so, the phenomenon of scalar mixing is numerically simulated with the goal of identifying some of the means by which non-Gaussian statistics are generated. The hope is to provide the reasons for these statistics as observed in recent laboratory and numerical experiments. The analysis is based on two computational procedures: (i) the mechanistic Linear Eddy Model (LEM) of Kerstein (1988), and (ii) DNS. The reasoning for the use of the LEM is its relative low computational cost, allowing a large number of simulations. It also provides a means of simulating high Reynolds number flows, albeit in a phenomenological manner. In the context considered, as will be described in the next section, LEM simulations reveal many features of scalar mixing which, in turn, identify several cases to be considered subsequently by DNS. In both simulations, only the transport of a passive and conserved scalar variable is considered; the analyses pertaining to dynamically active and/or chemically reactive scalars are postponed for future work.

2. Linear eddy model simulation

Details of the LEM and its application in modelling of turbulent mixing and chemical reaction are described in several papers by Kerstein (1988, 1989, 1990, 1991); for a recent review see McMurtry, Menon & Kerstein (1993*b*). The prominent feature of the model in applications to turbulence simulations is its capacity to explicitly differentiate among the different physical processes of turbulent stirring

† Not including the extensive literature of chemical engineering devoted to liquid scalar mixing (Brodkey 1975), since small-scale intermittency is not discussed in this literature.

(convection) and molecular diffusion (and chemical reaction). This is achieved by a reduced 'one-dimensional' (linear) description of the scalar field which allows the resolution of all length scales even for flows with relatively large Reynolds numbers. The physical interpretation of the one-dimensional domain is dependent on the particular case under consideration (Kerstein 1992). Along the one-dimensional domain, the diffusion process is implemented deterministically by the solution of the appropriate diffusion equation. The manner by which turbulent convection is treated constitutes the primary feature of the model. This process is modelled by random 'rearrangement' (stirring) events of the scalar field along the domain. The rules by which these rearrangement processes occur are established such that the random displacements of fluid elements result in a diffusivity that is equal to the 'turbulent diffusivity' of the flow. The parameters which govern this process are λ, the frequency of stirring, and $f(\ell)$, the p.d.f. of eddy size (ℓ) of the segments of the flow which are to be rearranged. To determine explicit expressions for the size and frequency of rearrangement events, a particular rearrangement *mapping* must be chosen. Kerstein (1991) shows that the *triplet* map reflects several physical features which suggest its choice for high Reynolds number turbulence simulations. The stirring events induced by this mapping introduce a random walk of a marker particle on the linear domain. Based on high Reynolds number scaling laws, the diffusivity induced by all eddies up to some size l is assumed to scale as $D_T(l) \sim l^p$. The parameter p takes on the value 4/3 for inertial-range turbulence, but can be treated as a variable to study other assumed scalings. Based on these scaling arguments, it can be shown that the following relations must be satisfied (Kerstein 1991):

$$f(\ell) = \frac{5}{3} \frac{\ell^{-8/3}}{\eta^{-5/3} - L_u^{-5/3}}, \quad \eta \leqslant \ell \leqslant L_u. \tag{1}$$

$$\lambda = \frac{54}{5} \frac{1}{L_u \tau_L} \left(\frac{L_u}{\eta} \right)^{5/3}. \tag{2}$$

Here, τ_L is the eddy turnover time, L_u is the integral scale and η is the Kolmogorov length scale. In this representation, the statistics of the velocity field are inputs to the model. The required model parameters which describe the turbulent field include the turbulent diffusivity (D_T), the integral velocity length scale (L_u), the Reynolds number (Re) and the Schmidt number (Sc). The relation between the model D_T and turbulent diffusivity is needed to relate the computational time to the physical time. The parameter L_u is defined as the largest allowable eddy for a given flow, and l represents the size of a 'typical' eddy. The LEM analogue of the Reynolds number is defined by $Re = (L_u/\eta)^{4/3}$. Equations (1) and (2) are based on scaling relations for high Reynolds number flows (Tennekes & Lumley 1972) and therefore the results are most applicable under this condition.

In the implementation of the model for the simulation of a three-dimensional homogeneous turbulent flow, the linear dimension is interpreted to be the time-varying space curve which is locally aligned with the prominent direction of the scalar gradient (Kerstein 1991). In the implementation of the triplet mapping (or any other mapping procedures), however, one must be careful about the magnitudes of the length scales involved in the simulations. For example, if the size of the whole computational domain (L_B) is small, the statistics are dependent on the mapping procedure. Moreover, the number of grid points employed for numerical discretization must be large enough to resolve the Kolmogorov scale sufficiently. Finally, the

Case	Initial condition for the scalar field	L_u	Re	Sc
LEM-1	Square wave, $L_\phi = 1$	1	90	0.7
LEM-2	Square wave, $L_\phi = 2$	1	90	0.7
LEM-3	Double square wave, $L_\phi = 1, 2$	1	90	0.7
LEM-4	Square wave, $L_\phi = 1$	3	90	0.7
LEM-5	Square wave, $L_\phi = 2$	3	90	0.7
LEM-6	Double square wave, $L_\phi = 1, 2$	3	90	0.7
LEM-7	Gaussian spectrum, $K_s = 2$	1	90	0.7
LEM-8	Gaussian spectrum, $K_s = 3$	1	90	0.7
LEM-9	Gaussian spectrum, $K_s = 8$	1	90	0.7
LEM-10	Gaussian spectrum, $K_s = 3$	2	90	0.7
LEM-11	Top-hat spectrum, $K_s = 2$	1	90	0.7
LEM-12	Top-hat spectrum, $K_s = 3$	1	90	0.7
LEM-13	Top-hat spectrum, $K_s = 8$	1	90	0.7
LEM-14	Double top-hat spectrum, $K_{s1} = 2, K_{s2} = 12$	1	90	0.7
LEM-15	Double top-hat spectrum, $K_{s1} = 8, K_{s2} = 12$	1	90	0.7
LEM-16	Double top-hat spectrum, $K_{s1} = 2,\ K_{s2} = 12$	2	90	0.7
LEM-17	Gaussian spectrum, $K_s = 20$	1	90	0.7
LEM-18	Gaussian spectrum, $K_s = 30$	1	90	0.7
LEM-19	Double square wave, $L_\phi = 1,\ 2$	1	50	0.7
LEM-20	Double square wave, $L_\phi = 5,\ 10$	5	900	0.7
LEM-21	Double square wave, $L_\phi = 1,\ 2$	1	90	0.05
LEM-22	Double square wave, $L_\phi = 1,\ 2$	3	90	0.05

TABLE 1. Conditions for the LEM simulations. For the cases denoted 'square wave', the initial scalar p.d.f. is an approximate double-delta function (equation (3)). For all the other cases, the initial p.d.f. is approximately Gaussian. In all the cases, $L_\phi = 1$ corresponds to 200 grid points. $K_s = 1$ corresponds to 1000 grid points. $L_u = 1$ corresponds to 200 grid points.

accuracy of the flow statistics is dependent on the number of grid points and the number of realizations employed for data sampling.

LEM results

The resolution requirement for the LEM simulations depends on the magnitudes of the model Reynolds number and the Schmidt number. As we shall see in the simulated results here, the outcome of mixing is strongly dependent on the length scales of the velocity and the scalar field. All the simulations are conducted within relatively large box sizes; typically, $N_c = L_B/L_u = O(100)$, where N_c denotes the number of 'cells' within the box. The number of grid points within each cell is determined in such a way to resolve the Kolmogorov length scale. McMurtry *et al.* (1993*a*) suggest that ≈ 6 grid points provide the sufficient resolution. For example, with $L_u = 1$ and $Re = 90$, with 200 grid points within each cell the desired accuracy is achieved. With this, there would be a total of $N = 200 \times N_c$ grid points within the whole domain. In addition, each simulation is repeated N_s times; thus the total number of samples for statistical analysis is $N_s \times N$. In most of the simulations, $N_c = 200$ is used. Simulations with smaller box sizes consisting of $N_c = 100$ cells yield almost identical results. In almost all the cases, the simulations are repeated $N_s = 100$ times. Therefore, the statistical information is gathered from 4×10^6 samples. The computer time to gather this many samples for $Re = 90$ simulations is about one hour on the Cray-YMP computer. While this is substantially less than that required for typical DNS (Givi 1994), it is not insignificant. Therefore, in some cases the magnitude of N_s was decreased but it was never less than 10. In order to mimic different mixing scenarios, a variety of different initial scalar

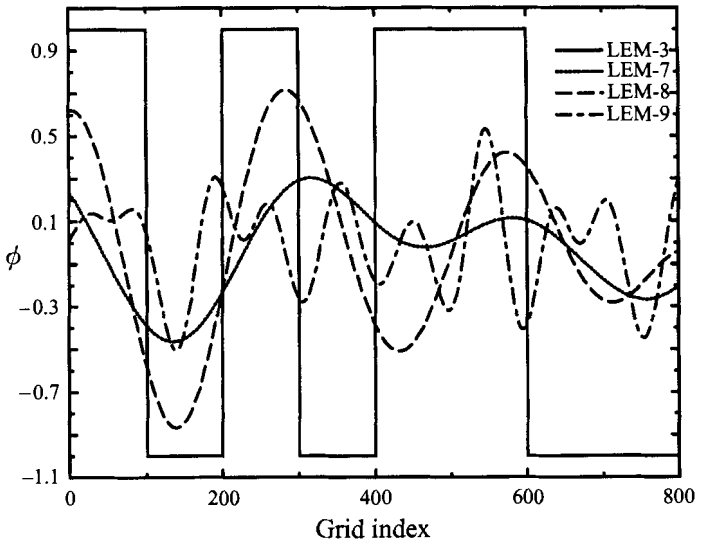

FIGURE 1. Initial distribution of the scalar for some of the LEM cases within a domain consisting of 800 grid points.

conditions are considered. All the cases considered are listed in table 1 and will be described in detail below. In all these cases, a stationary (non-decaying) hydrodynamic field is considered and its influence is modelled by the triplet mapping. The scalar field in all the cases is decaying. In addition to the initial distributions of the scalar field, the difference between the cases is due to the magnitudes of the hydrodynamic and the scalar length scales, the Schmidt number and the Reynolds number.

An objective of these LEM simulations (and also the DNS to be discussed in the next section) is to determine the time-evolution of the scalar statistics. There is no rigorous mathematical definition of the asymptotic time denoting the 'final' stage(s) of mixing (Kerstein & McMurtry 1994*a*). As mixing proceeds, the p.d.f. of the scalar field tends to form a delta function in the composition domain centred at the average value of the scalar, i.e. $P(\phi) \rightarrow \delta(\phi - \langle\phi\rangle)$; $\langle\phi\rangle$ denotes the ensemble-average value of the scalar variable ϕ with p.d.f. $P(\phi)$. At large times, the magnitude of the scalar variance σ^2 is significantly reduced ($\sigma^2 \rightarrow 0$ for a decaying scalar field) and the values of all constituents of the statistical ensemble are close to the mean scalar value. Here, the simulations are continued until the scalar variance decays to at least $O(10^{-3})$ of its initial value.

In the first set of simulations (LEM-1–LEM-3) the mixing progression from an initial condition corresponding to two scalar 'slabs' with alternating values of $\phi = \pm 1$ is considered. With this, the initial p.d.f. is composed of two delta functions:

$$P(\phi, t = 0) = \tfrac{1}{2}\delta(\phi - 1) + \tfrac{1}{2}\delta(\phi + 1). \tag{3}$$

In LEM-1 and LEM-2, the initial field is composed of a 'square wave', with wavelengths $L_\phi = 1$ and $L_\phi = 2$, respectively. In LEM-3, the initial field is composed of a 'double square wave' with $L_\phi = 1,\ 2$. In all three cases, $L_u = 1$. Figure 1 shows the double square wave distribution within a supercell as produced in LEM-3. The single square wave distribution, as used in LEM-1, is the same as that shown within the first 400 grids on this figure and is repeated throughout the domain. Cases LEM-4–LEM-6 employ the same scalar initializations as in LEM-1–LEM-3, respectively, but with $L_u = 3$.

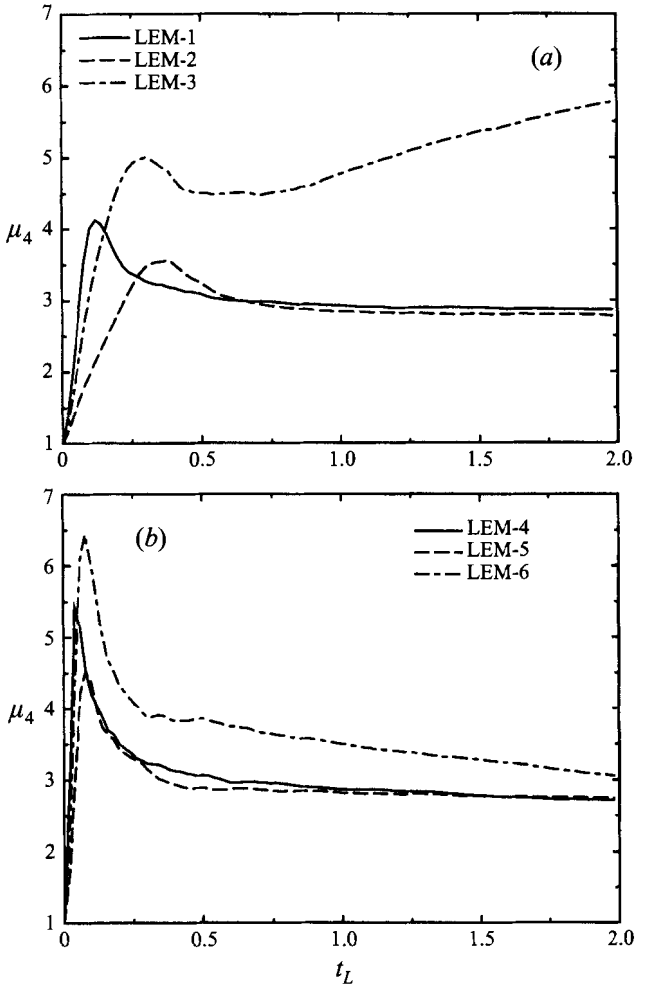

FIGURE 2. Temporal variation of the LEM-generated scalar kurtosis. The scalar field is initialized in the physical domain: (*a*) LEM-1 ($L_u = 1, L_\phi = 1$), LEM-2 ($L_u = 1, L_\phi = 2$), LEM-3 ($L_u = 1, L_\phi = 1, 2$); (*b*) LEM-4 ($L_u = 3, L_\phi = 1$), LEM-5 ($L_u = 3, L_\phi = 2$), LEM-6 ($L_u = 3, L_\phi = 1, 2$).

The temporal variations of the scalar kurtosis, μ_4 ($\mu_m = \langle \phi'^m \rangle / (\sigma^2)^{m/2}$, the prime denoting the deviation from the mean), in LEM-1–LEM-6 are shown in figure 2. A unit of time in these and all the subsequent figures pertaining to LEM simulations corresponds to one eddy turnover time, i.e. $t_L = t/\tau_L$. Figure 2(*a*) shows that in LEM-1 and LEM-2, after $t_L = 0.6$, the p.d.f.s adopt an approximate Gaussian distribution whereas in LEM-3 the p.d.f. exhibits tails broader than Gaussian. By increasing the hydrodynamic length scale (figure 2*b*) the behaviour in LEM-4 and LEM-5 show a similar trend. However, in LEM-6 the departure from Gaussian is significantly less than that in LEM-3. The p.d.f.s at $t_L = 2$ for these six cases are shown in figure 3, and the temporal variations of the correlation between the scalar and its rate of dissipation (ϵ_ϕ), defined by

$$\rho(t) = \frac{\langle \phi'^2 \epsilon_\phi \rangle}{\langle \phi'^2 \rangle \langle \epsilon_\phi \rangle} - 1 \tag{4}$$

are shown in figure 4. For a Gaussian distribution, ϕ and ϵ are statistically independent

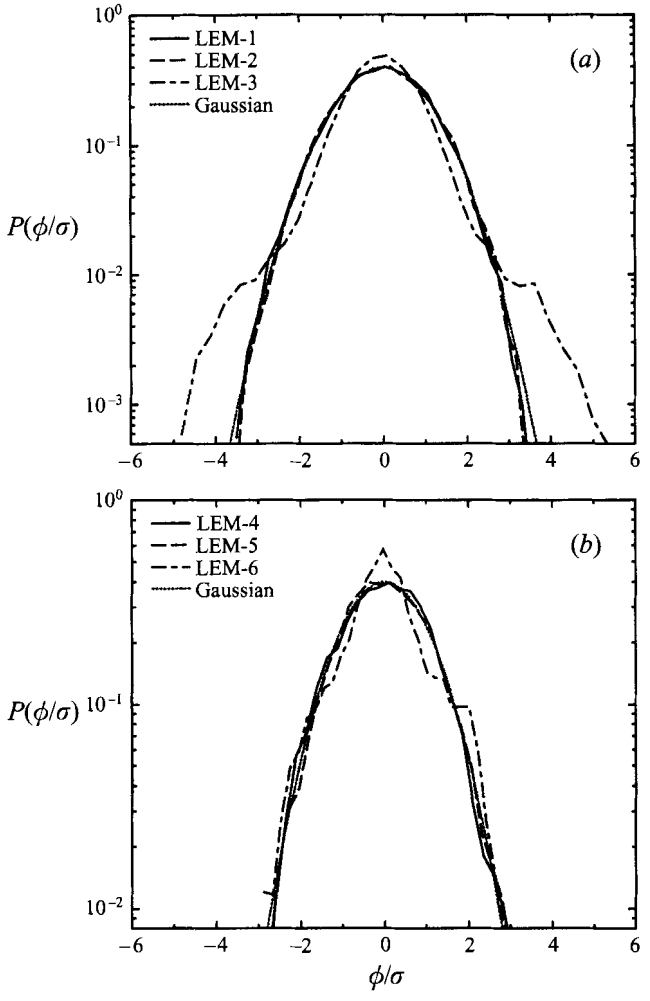

FIGURE 3. LEM-generated p.d.f.s of scalar at $t_L = 2$. LEM-1–LEM-6 as figure 2.

($\rho = 0$). Thus, the numerical values of ρ at large times provide an accurate measure of the deviation of the p.d.f. from Gaussian as observed in figure 3.

Figures 2–4 illustrate one reason for the non-Gaussian behaviour of the scalar p.d.f.. In all the cases with a single value for L_ϕ the p.d.f. is Gaussian after $t_L \approx 0.6$ regardless of the magnitude of L_u. In these cases, the influence of the hydrodynamic field as mimicked by the LEM is similar on all scalar blobs. Thus, the larger slabs of the scalar are broken as a result of triplet mapping, and mixing is completed by diffusion at small scales. The breakage of the scalar blobs is statistically the same in all the slabs even though the rate is different depending on the magnitude of L_ϕ. In this way, the mixing behaviour is similar to that in the laboratory experiments of Miyawaki *et al.* (1974) and Tavoularis & Corrsin (1981*a*) which do in fact suggest Gaussian p.d.f.s. The behaviour in LEM-3 is markedly different, primarily due to a 'non-uniform' influence of the hydrodynamic field. In this case with $L_u = 1$, the effect of stirring is more dominant in the slabs with $L_\phi = 1$ than those with $L_\phi = 2$. This means that the molecular mixing acts at different time levels for different L_ϕ values. Thus, the 'local' influence of mixing is not the same in square waves with different wavelengths. Consequently, at

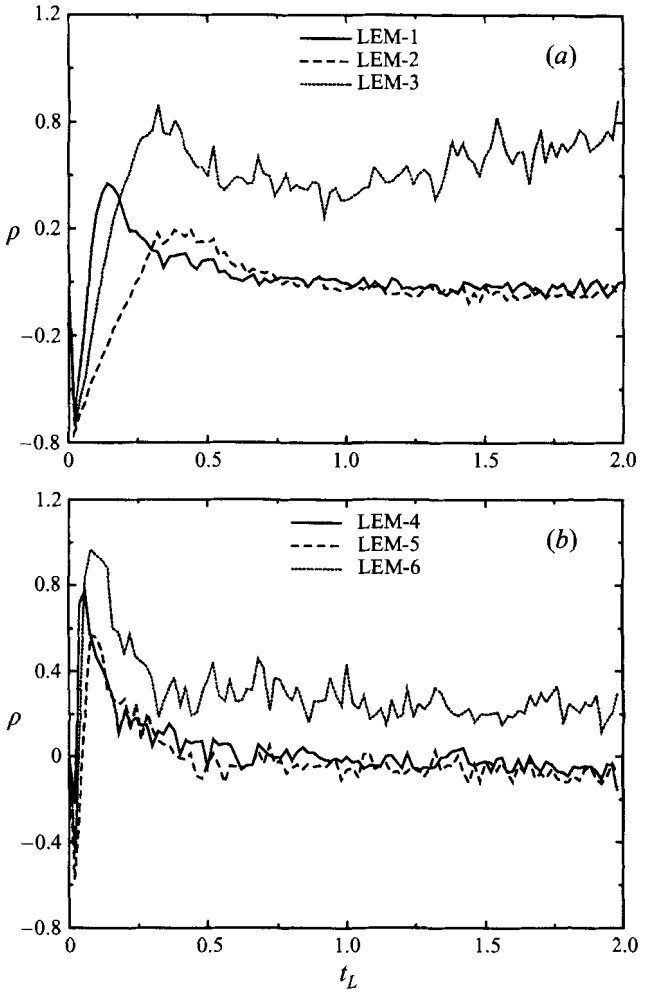

FIGURE 4. Temporal variation of LEM-generated ρ. LEM-1–LEM-6 as figure 2.

intermediate times the scalar fields are composed of 'two fields' whose combined weighted effects yield non-Gaussian statistics even if each of the two original fields are Gaussian. Although it is expected that a Gaussian p.d.f. would emerge if the computations are continued until very long times, the non-Gaussian behaviour does prevail for a long time. In this regard, it is important to indicate that at $t_L = 1$ the magnitude of the variance in LEM-3 ($\sigma^2 = 5.74 \times 10^{-4}$) is smaller than that in LEM-2 ($\sigma^2 = 5.96 \times 10^{-4}$). But the p.d.f. in LEM-2 is Gaussian and that in LEM-3 is exponential.

By increasing the magnitude of the velocity length scale $L_u = 3$, the departure from Gaussian becomes less significant. In this case (LEM-6), the influence of stirring is relatively more uniform (as compared with that in LEM-3) in all the scalar blobs. The reason is that now large scalar slabs rapidly follow the turbulence cascade (enacted by the triplet mapping) and the initial field is stirred uniformly before the molecular diffusion can significantly influence the p.d.f.. Thus, after the formation of exponential p.d.f.s at intermediate times, the p.d.f. at long times becomes closer to Gaussian. With the argument presented above it is plausible to expect the p.d.f. at long times in LEM-6 to be somewhere between those in LEM-3 and LEM-1.

It would be interesting to examine the evolution of the mixing from an initial Gaussian state. This is done in LEM-7–LEM-18. In these cases, the initialization procedure is similar to that used in the DNS of Eswaran & Pope (1988). It involves the specification of the scalar power spectrum with random magnitudes of the phase angles. This spectrum is specified within a subdomain (supercell) composed of 1000 grid points and the initial scalar field in each of the supercells is similar. For a box with 40 000 grids, there are 40 supercells each composed of 5 cells. The corresponding Fourier wavenumbers within each of the subdomains is between $-500 \leqslant K \leqslant 500$. The energy is distributed at low wavenumbers with the following functional forms: (i) a Gaussian spectrum with a peak at K_s:

$$E_\phi(K, t=0) = \frac{32}{3}\left(\frac{2}{\pi}\right)^{1/2} \frac{K^4}{K_s^5} \exp\left\{-2\left(\frac{K}{K_s}\right)^2\right\}; \tag{5}$$

(ii) a top-hat spectrum centered at K_s with a width $\Delta K = \frac{1}{2}$,

$$E_\phi(K,0) = \begin{cases} 1 & \text{if } K_s - \Delta K \leqslant K \leqslant K_s + \Delta K \\ 0 & \text{elsewhere;} \end{cases} \tag{6}$$

(iii) a double-hat spectrum with peaks centered at K_{s1}, K_{s2} with a width $\Delta K = \frac{1}{2}$,

$$E_\phi(K,0) = \begin{cases} 1 & \text{if } K_{s1} - \Delta K \leqslant K \leqslant K_{s1} + \Delta K \text{ or } K_{s2} - \Delta K \leqslant K \leqslant K_{s2} + \Delta K \\ 0 & \text{elsewhere.} \end{cases} \tag{7}$$

The Gaussian spectrum with $K_s \geqslant 3$ generates a multi-scale initial scalar field, whereas the top-hat spectrum yields an approximate single length scale. Figure 1 provides a typical graphical visualization of the initial scalar distribution within a supercell as produced in LEM-7–LEM-9.

With an initial Gaussian scalar field, the combined influences of advection and diffusion can yield non-Gaussian scalar p.d.f.s (Kimura & Kraichnan 1993). This issue is considered here where the role of several parameters in causing exponential p.d.f.s is discussed. In figure 5 results are presented of the temporal variations of the kurtosis for LEM-7–LEM-10 with initial Gaussian scalar fields. In LEM-7 with $K_s = 2$ the scalar field is primarily composed of large uniform size slabs. Therefore all the slabs are broken into smaller ones almost simultaneously. As a result, the kurtosis increases slowly then returns to the Gaussian value of 3. By distributing the initial energy around $K_s = 3$ (LEM-8), a wider range of the initial scalar length scales are produced with some of the scalar slabs larger than L_u. The evolution of the scalar kurtosis in this case portrays a roughly similar trend as that in LEM-3 (or LEM-6). The initial degree of segregation is, however, different. In LEM-8 the p.d.f. becomes exponential with tails broader than Gaussian even at very long times. An increase to $K_s = 8$ (LEM-9) does not necessarily enhance the behaviour. Although in this case the initial scalar field is composed of blobs with multiple length scales, most of the length scales are smaller than L_u. Thus the 'flapping' induced by the velocity field is dominant only at initial times when the kurtosis is slightly increased before the p.d.f. returns to the Gaussian state. A similar behaviour is observed for $K_s = 3$ with $L_u = 2$ (LEM-10).

A similar qualitative kurtosis evolution is observed for the cases with the initial top-hat spectrum (LEM-11–LEM-13) as shown in figure 6. However, in none of these cases do exponential p.d.f.s persist. This is due to the relative uniformity of the initial length scale distribution of the scalar. Thus the behaviour in all these cases is similar to those with a square wave distribution (e.g. LEM-1, LEM-2). However,

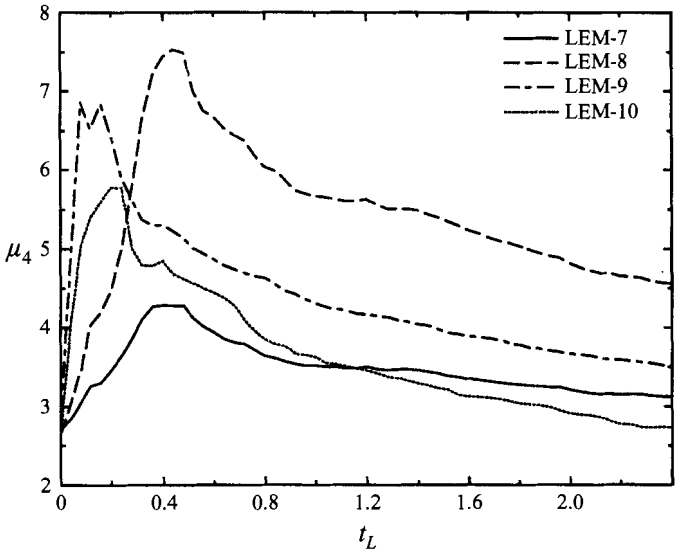

FIGURE 5. Temporal variation of the LEM-generated scalar kurtosis. The scalar field is initialized with a Gaussian spectrum: LEM-7 ($K_s = 2$, $L_u = 1$), LEM-8 ($K_s = 3$, $L_u = 1$), LEM-9 ($K_s = 8$, $L_u = 1$), LEM-10 ($K_s = 3$, $L_u = 2$),

when a double-hat spectrum is employed (LEM-14), a somewhat more profound non-Gaussian p.d.f. is observed. In this case, with $K_{s1} = 2, K_{s2} = 12$ the behaviour is similar to that in LEM-3 in which the approximate double length scale in the initial scalar field with $L_u = 1$ causes a persistent exponential p.d.f.. The increase of K_{s1} to 8 (LEM-15) or the increase of L_u to 2 (LEM-16) results in p.d.f.s closer to Gaussian. The reason for this behaviour is made clear by realizing that the conditions in LEM-15 and LEM-16 are 'effectively' similar to those in LEM-9 and LEM-10, respectively.

Another means of producing non-Gaussian behaviour is through the simultaneous interaction of velocity and scalar fluctuations at small scales. This issue will be discussed further in the next section where the DNS-generated results are discussed. At this point it suffices to present the results for LEM-17 and LEM-18. These correspond to mixing with an initial Gaussian spectrum but with $K_s = 20, 30$, respectively. In figure 7 the kurtosis evolutions for these cases are compared with that of LEM-9. This comparison indicates that by increasing the relative weight of the small scales the p.d.f.s develop flatter tails at early times. At long times, the kurtosis in LEM-17 ($K_s = 20$) is smaller than that in LEM-9. This is in accord with the trend shown in figure 5 for LEM-8 and LEM-9 which suggests that as K_s becomes larger the statistical behaviour becomes closer to Gaussian. However, by increasing K_s further to the value of 30, an increase in the kurtosis value is observed. Note that in this case, the initial length scale of the scalar field is much smaller than L_u. The triplet mapping implements velocity scales in the range $\eta \leqslant l \leqslant L_u$. The interactions of small scalar length scales with the velocity at small l values yield an overall non-Gaussian behaviour. It is noted that the departure from Gaussian as generated by the second mechanism is not very strong at long times.

Based on the results presented thus far, two scenarios are identified for causing non-Gaussian flat-tail scalar p.d.f.s. (i) When there is a separation of length scales in the initial condition of the scalar, and the dominant scale of advection is less than

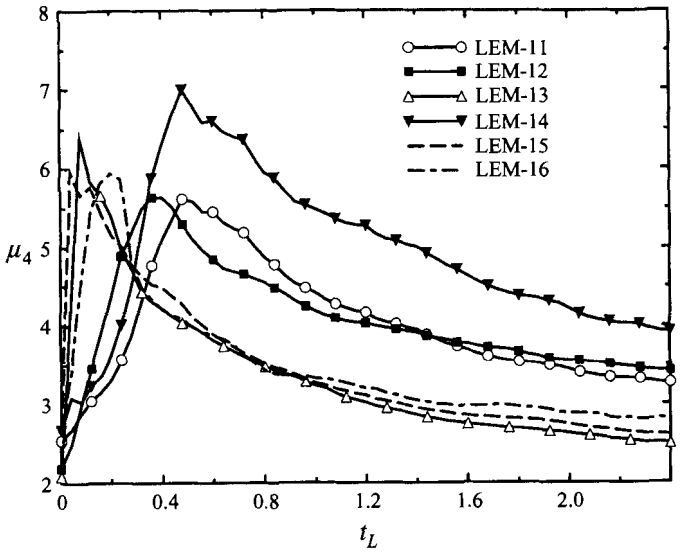

FIGURE 6. Temporal variation of the LEM-generated scalar kurtosis. The scalar field is initialized with a top-hat or a double-hat spectrum: LEM-11 ($K_s = 2$, $L_u = 1$), LEM-12 ($K_s = 3$, $L_u = 1$), LEM-13 ($K_s = 8$, $L_u = 1$), LEM-14 ($K_{s1} = 2$, $K_{s2} = 12$, $L_u = 1$), LEM-15 ($K_{s1} = 8$, $K_{s2} = 12$, $L_u = 1$), LEM-16 ($K_{s1} = 2$, $K_{s2} = 12$, $L_u = 2$),

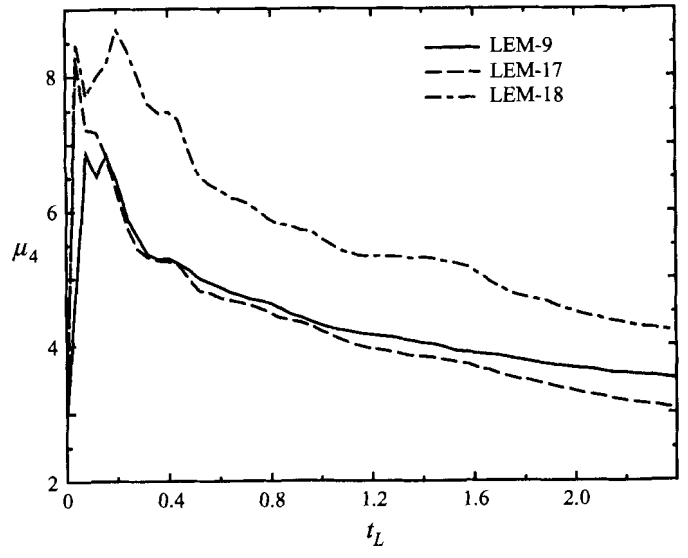

FIGURE 7. Temporal variation of the LEM-generated scalar kurtosis. The scalar field is initialized with a Gaussian spectrum: LEM-9 ($K_s = 8$, $L_u = 1$), LEM-17 ($K_s = 20$, $L_u = 1$), LEM-18 ($K_s = 30$, $L_u = 1$).

that of the scalar: in this case, the simultaneous action of advection and molecular diffusion causes the scalar to develop a non-Gaussian flat-tail p.d.f.. (ii) When there is an increase of the initial weight of small scales: in this case, the decrease in the magnitude of the scalar gradient occurs faster by the action of molecular diffusion. While the advection tends to drive the scalar-gradient p.d.f. toward a non-Gaussian form, molecular diffusion acts to return it to Gaussian. With a combination of these two effects, the scalar tends to be correlated with its gradient, thus a non-Gaussian

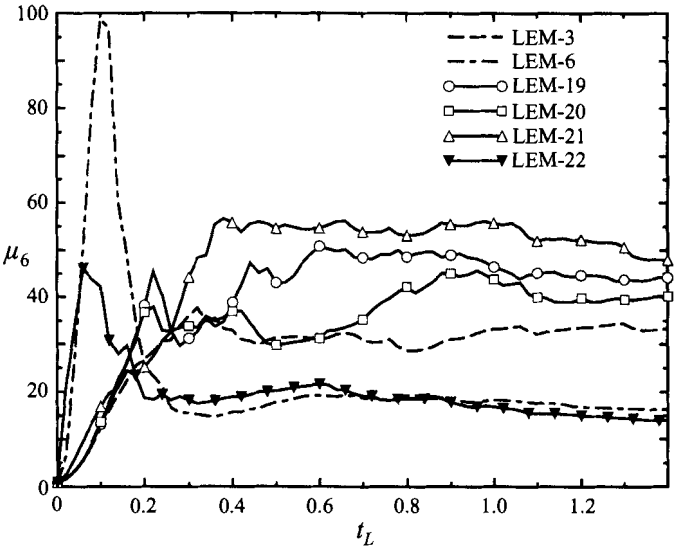

FIGURE 8. Temporal variation of the LEM-generated scalar superskewness. The scalar field is initialized in the physical domain as double square waves: LEM-3 (Re = 90, Sc = 0.7), LEM-6 (Re = 90, Sc = 0.7), LEM-19 (Re = 50, Sc = 0.7), LEM-20 (Re = 900, Sc = 0.7), LEM-21 (L_u = 1, Re = 90, Sc = 0.05), LEM-22 (L_u = 3, Re = 90, Sc = 0.05).

(usually flatter tail) p.d.f. develops. Note that the mechanism responsible for this non-Gaussian behaviour always exists. But when the initial weight of the small scales is large, the effects are more pronounced and are more clearly exhibited. In the cases considered here, the non-Gaussian behaviour generated by the first mechanism appears much stronger than that caused by the second route (compare, for example, LEM-18 with LEM-3).

At this point it is instructive to examine the influence of the model Reynolds number and the molecular Schmidt number on the outcome of mixing. While a thorough parametric study is not intended, cases LEM-19–LEM-22 provide some useful insight. In figure 8 results are presented of the temporal evolution of the scalar superskewness for the field initialized the same as in LEM-3 but with different values of the Reynolds and the Schmidt numbers. This figure shows that the overall influence of Re is not significant. This is to be expected, as in the context of the LEM the primary influence of the Reynolds number is on the variation of the velocity length scales participating in the rearrangement event. The influence of Sc is more intriguing. Figure 8 indicates that for the initial field composed of a double square wave with L_u = 1, a decrease in Sc yields a more pronounced exponential p.d.f. at long times, but it does not yield a noticeable influence when L_u = 3. The enhanced non-Gaussian behaviour at lower Sc values is not in accord with the expectation that the intermittency of the scalar derivative and the departure from Gaussian scalar p.d.f. increase with increasing Sc (Kerr 1985; McMurtry *et al.* 1993*a*). To explain the behaviour here, it is important to realize that in the absence of molecular diffusion the p.d.f. would not experience any changes. Therefore, as the magnitude of the molecular diffusion coefficient is increased, i.e. as Sc is decreased, the influence of molecular action on the p.d.f. becomes more pronounced. This influence is more noticeable when L_u = 1. In this case, the length scale of the velocity field is smaller than the largest scale of the scalar field. This velocity field influences the small scalar scales significantly but does not have a pronounced effect on the large scalar scales. As

Sc decreases, the difference between mixing of small-scale and of large-scale scalars becomes more significant. This yields a more exponential p.d.f. as demonstrated by the deviation of the results in LEM-21 from those in LEM-3. However, as the magnitude of the velocity length scale increases, the relative influence of advection (on the small- and the large-scale scalars) is similar and the p.d.f. at long times is not significantly modified. This is demonstrated by the similarity of the results in LEM-6 and LEM-22.

The results presented above can be better understood by considering the following physical scenario: consider two scalar blobs, one with a size smaller than the largest velocity eddy and the other blob larger than this eddy. As a result of advection, the small blob is almost immediately stirred by turbulence and follows the cascade down to small scales. The time scale of this process is the same as that of the turbulent diffusivity. In the same time period, the larger blob is only dispersed and 'waits' until its size becomes the same or smaller than that of the largest eddies. Then, it experiences a mixing similar to that felt by the smaller blob. Again, remember that molecular diffusion is only effective at small scales and the p.d.f. can only be changed with the presence of molecular diffusion. Therefore the p.d.f. corresponding to the small blob is now changed from an initial double delta to a mixed near-Gaussian form. The same would happen for the p.d.f. of the large blob but with a time lag. The weighted sum of the two statistics can behave in a variety of different forms depending on the weights of the two original blobs. At intermediate times, there will always be a combination of small and large scales as figure 8 does indicate strong non-Gaussian behaviour at intermediate times in all the cases. For the small blobs which are already stirred, molecular diffusion is more active and changes the p.d.f. more rapidly. During this change, the larger blobs wait until turbulence brings their sizes near to the active scales of molecular diffusion. Different statistics for different blobs imply, as indicated before, that the weighed sum of statistics exhibits stronger departure from Gaussian. Now if the size of the velocity eddy is larger than the largest of the scalar blobs, both blobs follow the turbulence cascade. During the time that molecular diffusion acts to change the p.d.f. from its double-delta form, the blobs are uniformly stirred by turbulence. Thus, the decrease of Sc would not have a significant influence on mixing at long times. In fact, if L_u is large enough it may even have an opposite effect. That is, as Sc decreases, the molecular diffusion can damp the rate of kurtosis and superskewness growth. Therefore, it is concluded that the role of Sc is very sensitive to both the initial scalar scale distribution and the initial extent of mixing. Further numerical simulations with large Schmidt numbers are required for a more elaborate investigation of this issue.

3. Direct numerical simulation

The results of the LEM simulations provide the guideline in our further, and somewhat more extensive, analysis of the problem via DNS. One of the early applications of DNS in the problem of turbulent scalar mixing and reaction is due to Hill (1979) and since then such simulations have provided a very useful and effective means of capturing some of the physical aspects of this complex phenomenon (Kerr 1983, 1985, 1990; Givi & McMurtry 1988; Eswaran & Pope 1988; Leonard & Hill 1988, 1991, 1992; McMurtry & Givi 1989; Metais & Lesieur 1992; Madnia, Frankel & Givi 1992; Frankel, Madnia & Givi 1993; Miller *et al.* 1993, 1995; Frankel 1993); a recent review is available (Givi 1994).

Our objective in the simulations conducted here is to analyse the statistical behaviour of passive scalars in three-dimensional, solenoidal, homogeneous and isotropic

velocity fields. All simulations are performed within a triply periodic box flow by means of a spectral-collocation numerical scheme employing Fourier basis functions (Givi & Madnia 1993). The hydrodynamic field is initialized by a random three-dimensional fluctuating velocity with zero mean and with a specified spectral density function. A wide-band von Kármán spectrum is imposed. The velocity field is then allowed to evolve according to the Navier–Stokes equations for more than 10 eddy turnover times to reach to a 'self-similar' condition. This is considered as the initial condition for the scalar mixing. Simulations are conducted with both 'unforced' and 'forced' hydrodynamic fields. In the former, the turbulence field is decaying whereas in the latter a steady turbulence field is established. The forcing scheme requires the energy in the low wavenumbers to remain constant. In this way the magnitudes of the turbulent length and velocity scales, and thus the magnitude of the Reynolds number, remain approximately constant throughout the evolution. Further details can be found in Givi (1989).

The transport of the scalar field is considered under two conditions: a zero mean scalar gradient and a constant (non-zero) mean scalar gradient.† In the former, the variance of the scalar field monotonically decreases as mixing proceeds; in the latter the mean scalar gradient forces the variance to reach an asymptotic value after a transient time. In this case, in order to maintain periodicity in all directions the scalar field ψ is decomposed into a mean and a fluctuating part as

$$\psi(\boldsymbol{x}, t) = \mathscr{A} y + \phi(\boldsymbol{x}, t). \tag{8}$$

Here ϕ denotes the mean-subtracted scalar value and $\mathscr{A}$ is a constant denoting the magnitude of the mean scalar gradient. With this initialization the transport of the scalar fluctuation is governed by

$$\frac{\partial \phi}{\partial t} + \boldsymbol{V} \cdot \nabla \phi + \mathscr{A} v = \mathscr{D}_M \nabla^2 \phi, \tag{9}$$

where $\boldsymbol{V}$ is the velocity field, v is the y-component of the velocity vector along which the scalar gradient is imposed, and $\mathscr{D}_M$ is the molecular diffusion coefficient. This equation indicates that the mean scalar gradient acts like a 'source' term in the ϕ transport equation. It is the statistics of this field that are of importance. Moreover, when $\mathscr{A} \neq 0$, the statistics of the normalized variable $\phi/\mathscr{A}$ are expected to be similar at long times. This was verified numerically. All the cases considered are listed in tables 2 and 3. The simulations are conducted with the following three initialization schemes.

Scheme 1: The initial scalar field has a Gaussian p.d.f. and is specified in Fourier space. The amplitudes of the Fourier modes are selected based on a specified input energy spectrum. The weights of the real and the imaginary components of each Fourier mode are determined based on a random phase. With this, the initial scalar field adopts a Gaussian p.d.f. in the physical domain. The conditions in all the flows initialized in this manner are listed in table 2(*a*). Different forms of the initial scalar spectra are considered as indicated in the second column of table 2(*a*). In the cases with a double-hat spectrum, the parameter α is defined as

$$\alpha = \frac{E(K_{s1}, t = 0)}{E(K_{s2}, t = 0)}. \tag{10}$$

Scheme 2: The initial scalar field yields an approximate double-delta p.d.f.. The

† Hereinafter, a 'constant' mean scalar gradient implies a 'non-zero' gradient unless otherwise stated.

	Case	Initial scalar spectra	$\mathscr{A}$	Turbulence	Re_λ	Sc
(*a*)	DNS-1	Gaussian		Forced	58	0.5
	DNS-2	Gaussian		Decaying	58 to 18	0.5
	DNS-3	Gaussian		Forced	38	0.5
	DNS-4	Gaussian		Decaying	38 to 13	0.5
	DNS-5	Top-hat, $K_s = 1$		Forced	58	0.5
	DNS-6	Top-hat, $K_s = 5$		Forced	58	0.5
	DNS-7	Double-hat, $K_{s1} = 1, K_{s2} = 5, \alpha = 0.2$		Forced	58	0.5
	DNS-8	Double-hat, $K_{s1} = 1, K_{s2} = 5, \alpha = 1$		Forced	58	0.5
(*b*)	DNS-9	Top-hat, $K_s = 8$	0	Forced	58	0.5
	DNS-10	Double-hat, $K_{s1} = 1,\ K_{s2} = 8,\ \alpha = 0.125$	0	Forced	58	0.5
	DNS-11	Double-hat, $K_{s1} = 1,\ K_{s2} = 8,\ \alpha = 1$	0	Forced	58	0.5
	DNS-12	Double-hat, $K_{s1} = 1,\ K_{s2} = 8,\ \alpha = 0.125$	0	Both	58 to 18	0.5
	DNS-13	Double-hat, $K_{s1} = 1,\ K_{s2} = 8,\ \alpha = 1$	0.2	Forced	58	0.5
	DNS-14	Top-hat, $K_s = 8$	0.5	Forced	58	0.5
	DNS-15	Top-hat, $K_s = 1$	0.5	Forced	58	0.5
(*c*)	DNS-16	Square wave	0	Forced	58	0.5
	DNS-17	Double square wave	0	Forced	58	0.5
	DNS-18	Double square wave	0	Forced	58	0.05

TABLE 2. Conditions for 64^3 DNS. (*a*) Scheme 1 (with an initial Gaussian p.d.f.). Each of the simulations for DNS-1–DNS-4 are conducted under all of the following conditions: (I) $K_s = 8$, $\mathscr{A} = 0$, (II) $K_s = 4$, $\mathscr{A} = 0$, (III) $K_s = 1$, $\mathscr{A} = 0$, (IV) $K_s = 8$, $\mathscr{A} = 0.5$, (V) $K_s = 1$, $\mathscr{A} = 0.5$. In all the other simulations, $\mathscr{A} = 0$. (*b*) Scheme 2 (with an initial double-delta p.d.f.). In the case indicated 'both' in column 4 the flow is forced until $t_D = 3$. After this time, forcing is removed. (*c*) Scheme 3 (scalar field initialized in the physical domain).

scalar field is initialized in a more isotropic manner than that composed of square waves (Scheme 3). The procedure is essentially the same as that first proposed by Eswaran & Pope (1988). Again, the components of the Fourier scalar modes are specified by a random phase. These components are then transformed back into the physical space. The scalars with a negative amplitude are set to $\phi = -1$ and those with a positive value are set to $\phi = +1$. The numerical simulation of the field with this 'exact' double-delta distribution is not possible due to formation of very sharp gradients in the physical domain. This problem is overcome by transforming the scalar field into the Fourier domain and decreasing the relative weights at high wavenumbers. As a result, the physical values are no longer bounded by ± 1 (Eswaran & Pope 1988). This field is allowed to go through molecular diffusion to reduce the amplitude. In the simulations here the initial scalar values are bounded by ± 1.01. Table 2(*b*) provides the list of all the parameters employed in DNS of flows initiated by this scheme.

Scheme 3: The scalar field is initialized in the physical domain in such a way as to yield a square wave in the y-direction (Givi & McMurtry 1988). The scalar slabs with $\phi = \pm 1$ values are similar to those shown in figure 1 for LEM-1. To avoid sharp gradients in DNS, the scalar slab interfaces are prescribed by an error function. The scalar values are constant in (x, z)-planes in each of the locations along the y-direction. The flow parameters for the simulations with this initialization are listed in table 2(*c*).

The simulations of the cases listed in table 2 are conducted in a domain discretized by 64^3 Fourier-collocation points. In a few cases, listed in table 3, some simulations with 128^3 collocation points are also conducted. In some of the cases, the simulations are repeated several (up to 10) times to ensure the reliability of the statistics; the

Case	Scheme	Initial scalar field	$\mathscr{A}$	Turbulence	Re_λ	Sc
BDNS-1	3	Double square wave	0	Forced	80	0.5
BDNS-2	2	Double-hat, $K_{s1} = 1, K_{s2} = 8, \alpha = 0.125$	0	Forced	80	0.5
BDNS-3	1	Gaussian, $K_s = 8$	0.5	Forced	80	0.5

TABLE 3. Conditions for 128^3 DNS. For schemes 1 and 2 column 3 specifies the initial shapes of the spectral density function of the scalar. For scheme 3 column 3 specifies the initial scalar profile in the physical space.

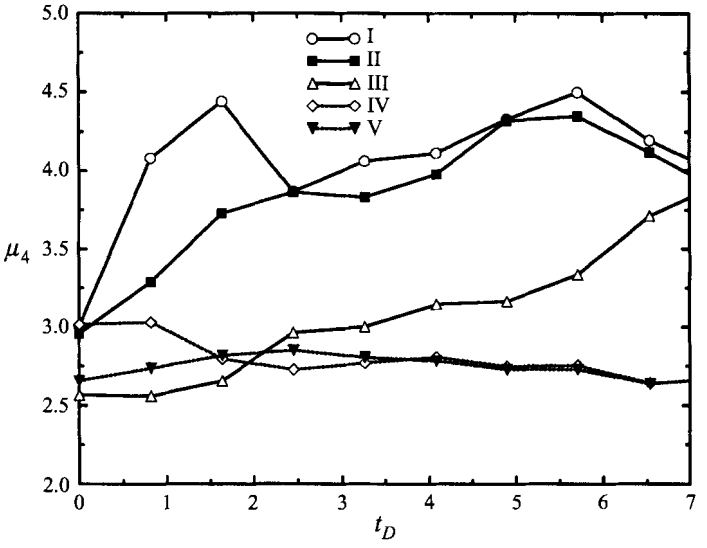

FIGURE 9. Temporal variation of the scalar kurtosis generated by DNS-1. Forced turbulence, $Re_\lambda = 58$, with an initial Gaussian spectrum and an initial Gaussian p.d.f. (Scheme 1): (I) $K_s = 8$, $\mathscr{A} = 0$, (II) $K_s = 4$, $\mathscr{A} = 0$, (III) $K_s = 1$, $\mathscr{A} = 0$, (IV) $K_s = 8$, $\mathscr{A} = 0.5$, (V) $K_s = 1$, $\mathscr{A} = 0.5$.

trends portrayed by the statistics are shown to remain similar. The definition of the other variables listed in tables 2 and 3 is clear. These variables indicate the presence ($\mathscr{A} \neq 0$), or the absence ($\mathscr{A} = 0$) of the mean scalar gradient, the dynamics of the velocity field (forced, decaying, or both), and the magnitudes of the Reynolds number based on the Taylor length scale (Re_λ) and the molecular Schmidt number (Sc).

DNS results

The 'time' t_D in the figures presented in this section denotes the time as normalized by the eddy turnover time of DNS. Since a variety of different conditions are considered, the magnitude of the eddy turnover time is not identical in all the simulations. In the cases with a decaying turbulence field, the initial eddy turnover time is used. It is important to indicate here that τ_L is an order of magnitude larger than τ_D (McMurtry *et al.* 1993*a*). In all of the cases described below, the field of velocity fluctuations exhibits a nearly Gaussian p.d.f.. The statistics of this field are not presented here; rather, the statistical behaviour of the scalar field is the subject of detailed discussions.

First, the mixing evolution from an initial Gaussian state (Scheme 1) is considered. As indicated in table 2(*a*), the difference between the cases is associated with the

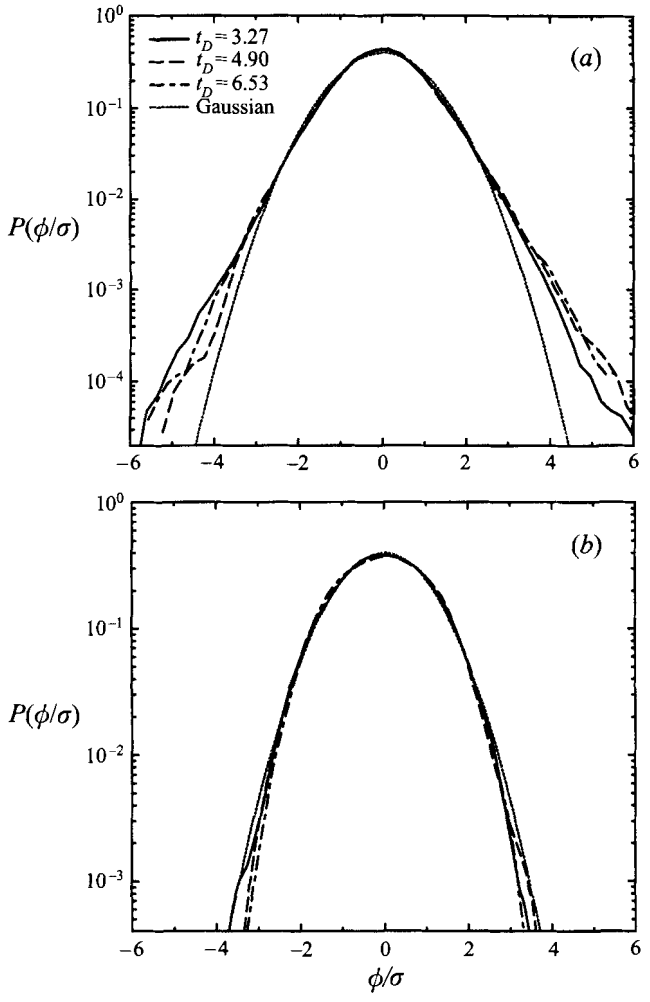

FIGURE 10. Normalized p.d.f.s of the scalar field at several time levels generated by DNS-1. (*a*) case I: $K_s = 8$, $\mathscr{A} = 0$; (*b*) case IV: $K_s = 8$, $\mathscr{A} = 0.5$.

magnitudes of K_s and $\mathscr{A}$. Each of the simulations for an initial Gaussian spectrum (DNS-1–DNS-4) is conducted under all of the following conditions: (I) $K_s = 8$, $\mathscr{A} = 0$; (II) $K_s = 4$, $\mathscr{A} = 0$; (III) $K_s = 1$, $\mathscr{A} = 0$; (IV) $K_s = 8$, $\mathscr{A} = 0.5$; (V) $K_s = 1$, $\mathscr{A} = 0.5$. In figure 9 the temporal evolution of the kurtosis for DNS-1, cases I–V is presented. To generalize the conclusions drawn from the scalars' kurtosis profiles, the variations of higher-order moments, the profiles of the p.d.f.s, the 'conditional expected dissipation' of the scalars, and the correlation between the scalar and its dissipation (equation (4)) are monitored in all the simulations. These statistics are useful for a quantitative description of the departure from Gaussian, especially at the tails of the p.d.f. (Sinai & Yakhot 1989; Miller *et al.* 1993; Jaberi, Miller & Givi 1995). However, with the exception of the p.d.f.s and some of the higher moments in some of the cases, these profiles are not shown. The results in figure 9 indicate that in I and II the p.d.f.s quickly develop exponential tails, whereas in IV and V they remain approximately Gaussian at all times. These are also observed in the p.d.f. profiles in figure 10 for cases I and IV. In III, the scalar field starts with

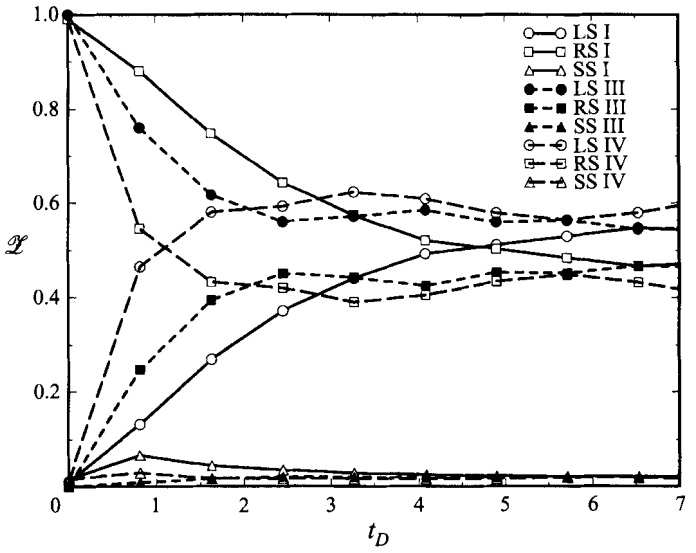

FIGURE 11. Temporal variation of the parameter $\mathscr{Z}$ generated by DNS-1. I: $K_s = 8$, $\mathscr{A} = 0$, III: $K_s = 1$, $\mathscr{A} = 0$, IV: $K_s = 8$, $\mathscr{A} = 0.5$.

mostly large length scales. Thus, the statistics remain Gaussian for a long time. In the presence of a constant mean gradient, the kurtosis varies slightly (IV, V) regardless of initial conditions. As expected, after the initial transient time the statistics become identical in these two cases. The trends observed in the first three cases can be explained in view of the LEM results. The initial field in case I is mostly composed of small scalar scales; thus the behaviour is somewhat similar to that in LEM-18. That is, the second mechanism for non-Gaussian behaviour, as identified above is observed. In III, the initial scalar field is dominated by large scales; thus the tendency for non-Gaussian behaviour is very weak for a long time. In case II, the initial field is composed of both small and large scalar scales and yields a relatively strong non-Gaussian behaviour similar to that observed in LEM-8.

A useful means of characterizing the influence of mixing is by band-pass filtering of the DNS data. Here, the whole band of the scalar spectrum in the range $0 < k < 30$ is divided into regions $0 < k \leqslant 3$, $3 < k \leqslant 15$, $3 < k \leqslant 30$, and $15 < k \leqslant 30$. At the ranges of the Reynolds numbers considered, the separation of scales in the physical domain cannot be represented by a Fourier band-pass cutoff. Nevertheless, we refer to these regions as those pertaining to large scales (LS), intermediate scales (IMS), retained scales (RS) and small scales (SS), respectively. The temporal variation of the 'percentage of the scalar energy' is defined as

$$\mathscr{Z}(t) = \frac{\int_{K_\ell}^{K_u} E_\phi(K,t)\mathrm{d}K}{\int_0^{K_{max}} E_\phi(K,t)\mathrm{d}K}, \tag{11}$$

where K_ℓ, K_u indicate the lower and the upper cutoff wavenumbers, respectively, and the denominator on the right-hand-side denotes the scalar variance. The corresponding $\mathscr{Z}$ values for some of the representative cases of DNS-1 are shown in figure 11. This figure indicates that in all the cases (some not shown for clarity) only a very small portion, typically less than 2%, of the total energy is associated with SS. In case I,

the magnitude of $\mathscr{Z}$ associated with LS increases and that of RS decreases, until the two become very close at $t_D \approx 4$. A similar trend is observed in II (not shown) but the initial difference between the LS and the RS values of $\mathscr{Z}$ are understandably less. Therefore, it takes a shorter time for the two $\mathscr{Z}$ values to become equivalent. In III, the $\mathscr{Z}$ values for LS are significantly greater than those for RS at initial times. Therefore, the statistics are expected to be dictated primarily by LS. In IV, the initial evolution of $\mathscr{Z}$ values is similar to those in I. However, within a very short time LS values become larger than those corresponding to RS. The results for V (not shown) are in accord with those here: at small times the profiles are similar to those in III and after $t_D \approx 2$ they become almost identical to those in IV. A striking feature portrayed by these results is the independence of the results at long time from the variance ratios at the initial time. Figure 11 indicates that despite a noticeable difference in the initial allocation of variances pertaining to LS and RS, the long-time ratios of the variances are very close. In fact, with the two cases with a mean gradient the results are almost identical. The kurtosis values of the filtered data are presented in figure 12. Part (*a*) of this figure indicates that the p.d.f.s associated with LS are nearly Gaussian at all times in all the cases. The IMS-p.d.f.s (figure 12*b*) are flatter than Gaussian, but the departure from Gaussian is less when a mean gradient is imposed. In all the cases, the kurtosis values associated with SS are consistently high (figure 12*c*), indicating exponential p.d.f.s for SS. These results indicate that while non-Gaussian behaviour can be developed within the full and the intermediate scales, it is not an inherent property of large scales. This observation is very useful in our discussions below.

Contrary to that of the scalar, the p.d.f. of scalar derivatives exhibits a somewhat similar behaviour in all the cases. In figure 13, results are presented of the p.d.f. of $\partial\phi/\partial y$ where it is shown that in all the cases an intermittent behaviour is prevailed. Moreover, the statistics are expected to be different when a mean scalar gradient is imposed. The results in figure 13 show symmetric p.d.f.s for cases I–III, but skewed p.d.f.s for IV and V. It has been established that a scalar field embedded in a locally isotropic velocity field may not be locally isotropic (Budwig, Tavoularis & Corrsin 1985; Thoroddsen & Van Atta 1992; Tong & Warhaft 1994). This is typically measured by the skewness of the scalar-fluctuation derivatives since, by reflectional symmetry they should all vanish if the scalar field is locally isotropic. The asymmetry of the p.d.f. in figure 13 is consistent with the experimental measurements (Van Atta & Antonia 1980; Tavoularis & Corrsin 1981*a*; Budwig *et al.* 1985; Thoroddsen & Van Atta 1992) and recent simulated results (Holzer & Siggia 1994; Pumir 1994; Miller *et al.* 1995). The mechanism responsible for the skewness is due to the mean scalar gradient, even though the velocity field is isotropic. The p.d.f.s of the scalar dissipation (not shown) exhibit departure from a log-normal distribution with a considerable skewness, consistent with the results of previous computational and experimental investigations (Eswaran & Pope 1988; Andrews & Shivamoggi 1990; Vincent & Meneguzzi 1991; Jayesh & Warhaft 1992; Miller *et al.* 1995).

The temporal evolution of the scalar kurtosis in DNS-2 (for cases I–V) with an unforced hydrodynamic field is shown in figure 14. A comparison of this figure with figure 9 reveals the significance of forcing. In case I, a mild increase in the kurtosis suggests that a non-Gaussian p.d.f. for this case is due to the interaction of diffusion and advection at small scales which is weaker than that in the stationary field (DNS-1). In II, the magnitude of the kurtosis increases (similar to that in DNS-1(II)), but the tendency to return toward the Gaussian state is very weak and the field retains its non-Gaussian state even at long times. The decay of turbulence energy is the primary factor in retaining the non-Gaussian p.d.f.. Again, in the presence of the

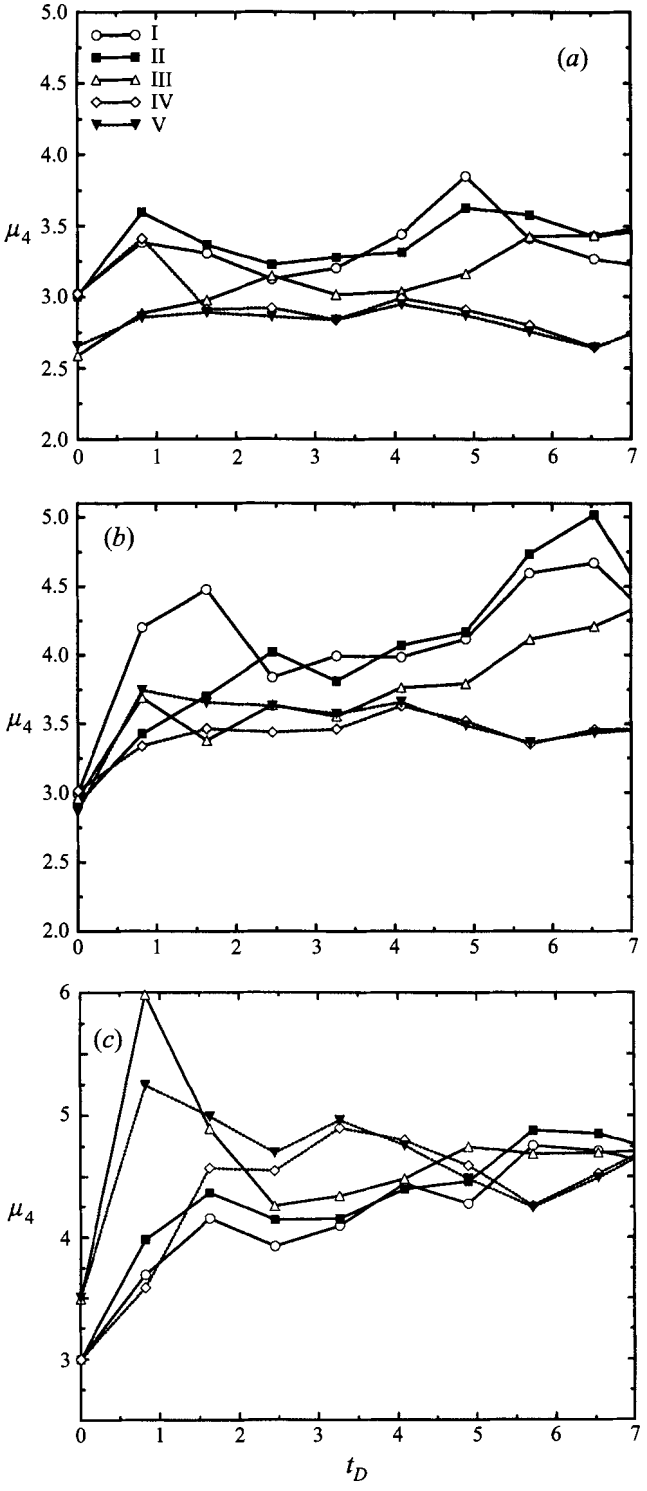

FIGURE 12. Temporal variation of the partitioned kurtosis generated by DNS-1. I: $K_s = 8$, $\mathscr{A} = 0$, II: $K_s = 4$, $\mathscr{A} = 0$, III: $K_s = 1$, $\mathscr{A} = 0$, IV: $K_s = 8$, $\mathscr{A} = 0.5$, V: $K_s = 1$, $\mathscr{A} = 0.5$. (*a*) LS ($0 < K \leqslant 3$), (*b*) IMS ($3 < K \leqslant 15$), (*c*) SS ($15 < K \leqslant 30$).

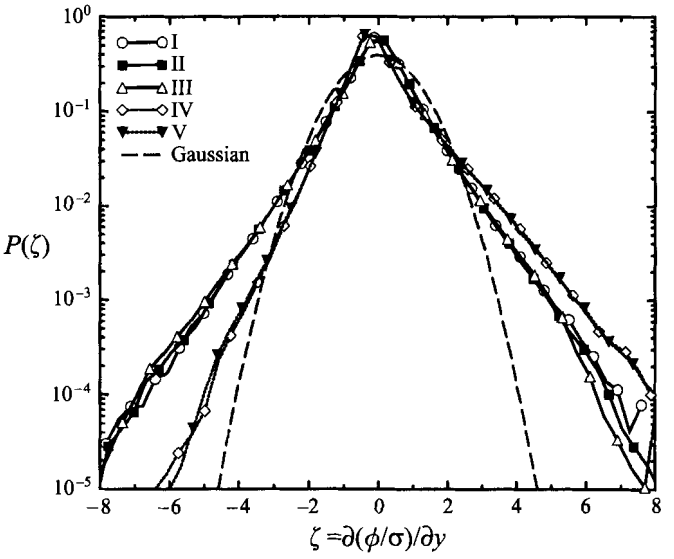

FIGURE 13. Normalized p.d.f.s of the scalar derivatives in the y-direction in DNS-1 at $t_D = 3$.

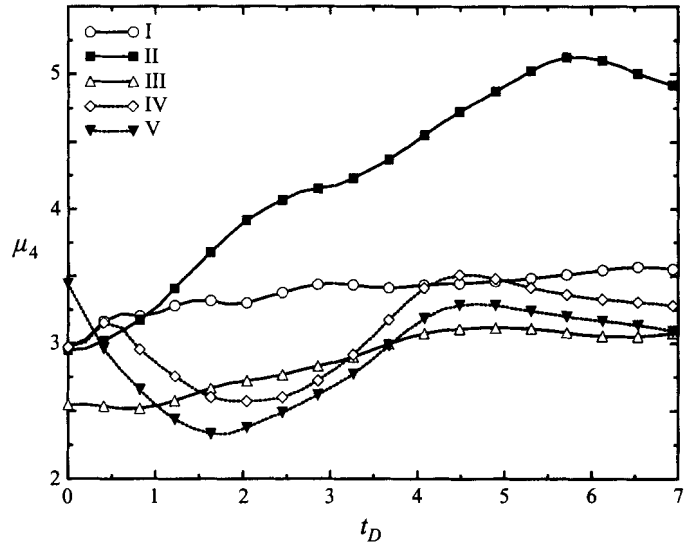

FIGURE 14. Temporal variation of the scalar kurtosis generated by DNS-2. Decaying turbulence, $Re_\lambda = 58$ to 18, with an initial Gaussian spectrum and an initial Gaussian p.d.f. (Scheme 1): (I) $K_s = 8$, $\mathscr{A} = 0$, (II) $K_s = 4$, $\mathscr{A} = 0$, (III) $K_s = 1$, $\mathscr{A} = 0$, (IV) $K_s = 8$, $\mathscr{A} = 0.5$, (V) $K_s = 1$, $\mathscr{A} = 0.5$.

mean gradient (cases IV and V) the statistics at long times are similar. However, it is noted that the extent of similarity is not the same as that in cases IV and V of DNS-1. This implies that in a decaying field with a mean scalar gradient, the effect of initial conditions can be more preserved than in a stationary field. This behaviour was consistently observed in all our other simulations and is useful in interpreting some of the experimental results, as will be discussed in the next section. The p.d.f.s of the y-derivative of the scalar (not shown) portray a trend similar to that in figure 13 indicating that skewed p.d.f.s are also formed in decaying (lower Re) flows.

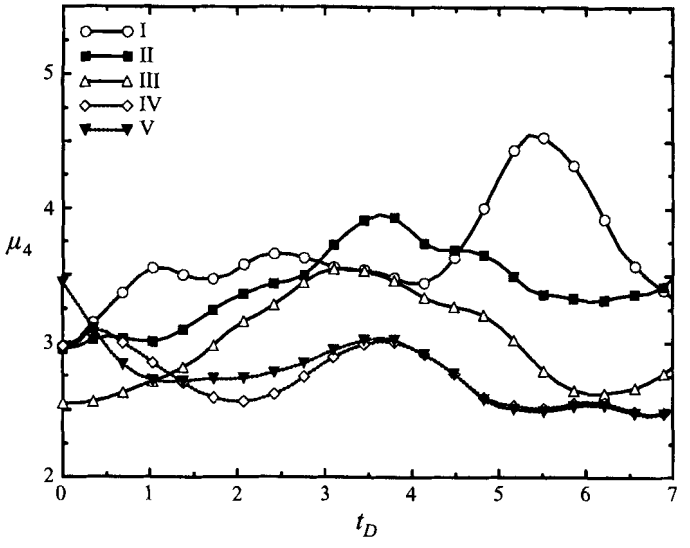

FIGURE 15. As figure 14 but generated by DNS-3. Forced turbulence, $Re_\lambda = 38$.

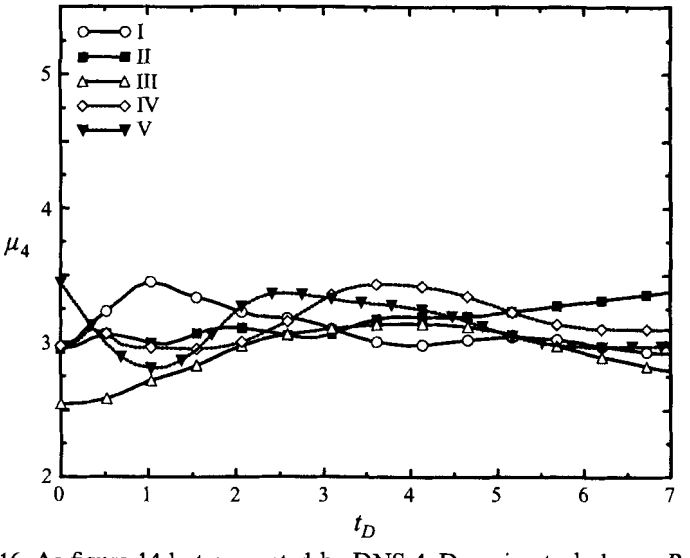

FIGURE 16. As figure 14 but generated by DNS-4. Decaying turbulence, $Re_\lambda = 38$ to 13.

A decrease in the magnitude of the Reynolds number is expected to yield a milder non-Gaussian behaviour. This is shown in figure 15 where results are presented for DNS-3. The Reynolds number in all the cases in DNS-3 is smaller than those in DNS-1. A comparison of this figure with figure 9 indicates that the initial growth rate of the scalar kurtosis is less when the Reynolds number is decreased. In case I, after a mild increase during four eddy turnover times, the kurtosis increases abruptly and then relaxes toward the Gaussian value. Again, in all the cases with the mean scalar gradient (cases IV and V) the scalar field remains Gaussian at all times. The influence of hydrodynamic forcing is more dominant at this lower Reynolds number, as the results for DNS-4 in figure 16 show that with a decaying turbulence field, no

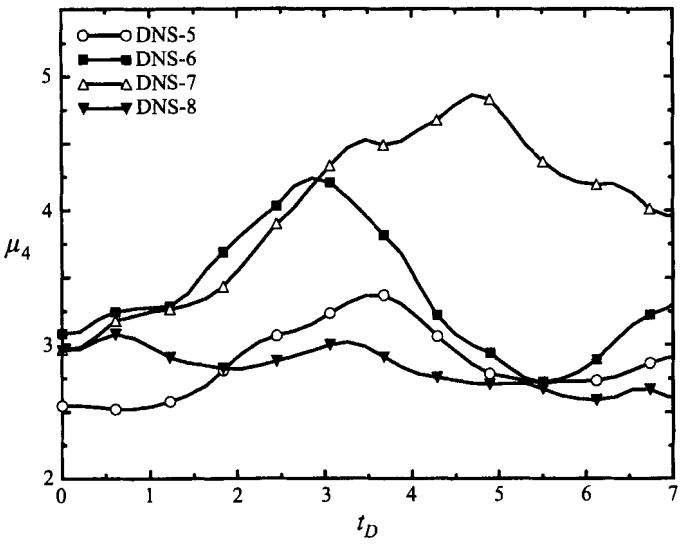

FIGURE 17. Temporal variation of the DNS-generated scalar kurtosis. Forced turbulence, $Re_\lambda = 58$. The scalar field is initialized with a top-hat or double-hat spectrum and an initial Gaussian p.d.f. (Scheme 1). DNS-5 ($K_s = 1$), DNS-6 ($K_s = 5$), DNS-7 ($K_{s1} = 1$, $K_{s2} = 5$, $\alpha = 0.2$), DNS-8 ($K_{s1} = 1$, $K_{s2} = 5$, $\alpha = 1$).

significant change is observed from the initial Gaussian scalar field (compare with figures 14 and 15).

Based on the results presented for DNS-1–DNS-4 it can be concluded that at moderate Reynolds numbers, the statistics of the scalar field with a zero mean scalar gradient are strongly dependent on the initial conditions. In the presence of a steady (forced) advection field, the scalar p.d.f. can change from an initial Gaussian to a highly non-Gaussian distribution depending on the initial weights of small- and large-scale scalars. If the turbulence field is allowed to decay, once a non-Gaussian p.d.f. develops it lasts longer. As the magnitude of the Reynolds number decreases it is still possible to develop non-Gaussian p.d.f.s although at a much later time. Now if, in addition, the turbulence field is allowed to decay, departure from the Gaussian state is further delayed (in our case it is never developed).

To further examine the effects of the initial scalar length scale distribution on the long-time statistics, the results for DNS-5–DNS-8 are considered in figure 17. In DNS-5 and DNS-6, the scalar field is initialized with a Gaussian scalar p.d.f. and a top-hat energy spectrum. The results for these two cases indicate that, in accord with the LEM results (LEM-9, LEM-18), by increasing the magnitude of K_s the kurtosis adopts higher values at intermediate times. By adding a small amount of energy at large scales the non-Gaussian behaviour can be significantly enhanced. This is witnessed in DNS-7 in which the initial field is similar to DNS-6 (with $K_{s2} = 5$) but with a relatively small energy ($\alpha = 0.2$) at $K_{s1} = 1$. In this case, the exponential behaviour is preserved throughout mixing. However, for large α values, e.g. DNS-8 in which the energy is distributed equally between wavenumbers 5 and 1, the growth of the kurtosis is significantly damped. In this case, the field is dominated by large scales and does not allow exponential p.d.f.s. The results for a case with $K_{s1} = 1$, $K_{s2} = 8$ show a similar behaviour, and thus are not shown. These observations are in accord with our earlier findings based on the LEM in that the presence of initial multi-length scalar scales results in departure from Gaussian if the initial energy is distributed

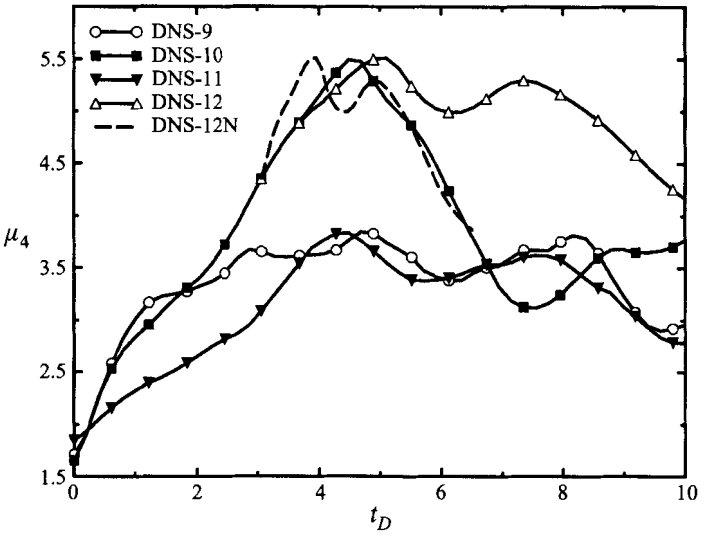

FIGURE 18. Temporal variation of the DNS-generated scalar kurtosis. The scalar field is initialized with a top-hat or double-hat spectrum and an initial double-delta p.d.f. (Scheme 2). DNS-9 ($K_s = 8$), DNS-10 ($K_{s1} = 1$, $K_{s2} = 8$, $\alpha = 0.125$), DNS-11 ($K_{s1} = 1$, $K_{s2} = 8$, $\alpha = 1$), DNS-12 ($K_{s1} = 1$, $K_{s2} = 8$, $\alpha = 0.125$). All cases are with a forced turbulent field. The forcing is removed at $t_D = 3$ in DNS-12. The case DNS-12N is the same as DNS-12 but the time axis is normalized by the effective eddy turnover time.

'appropriately' and the field is not dominated by large scales. By 'appropriate' it is meant that there is some energy at large scalar scales, but its magnitude is smaller than that at other scales. It is not at present possible to predict *a priori* the response to a specific α value in the range specified without conducting DNS.

The results for the cases with an initial double-delta p.d.f. (Scheme 2) are discussed next. The evolution of the kurtosis in DNS-9–DNS-12 is shown in figure 18. This figure shows that in contrast to the case with an initial Gaussian p.d.f., when the magnitude of energy in the small scales is relatively large (DNS-9), the kurtosis at long times is not significantly larger than 3. This suggests that starting from an unmixed scalar field, the increase of small scales does not necessarily yield non-Gaussian behaviour. By increasing energy by 12.5% at large scales (DNS-10) the kurtosis grows significantly and the p.d.f. develops exponential tails. However, at $t_D \approx 4.5$ the kurtosis starts to decrease rapidly and adopts a near-Gaussian value at long times. The reason for this return to the Gaussian state is that in this case the dominant scalar length scale is comparable to the hydrodynamic length scale. So, the exponential nature of the p.d.f. is rapidly destroyed by the stirring process (similar to LEM-6). This is further assessed in DNS-12. The initialization in this case is similar to that in DNS-10, but at $t_D = 3$ the forcing of the hydrodynamic field is removed. In this case, interestingly, the kurtosis decays very slowly and the exponential nature of the p.d.f. is preserved for a longer time. As before, by increasing the energy at large scales (DNS-11) the growth of the kurtosis is damped and the p.d.f. remains close to Gaussian. A comparison of the results for cases DNS-10 and DNS-12 suggests that once an exponential p.d.f. is established it has less tendency to relax when the turbulent field is decaying. The difference between DNS-10 and DNS-12 can be roughly related to the difference in the magnitudes of the eddy turnover times due to the difference in the advection fields in the two simulations.

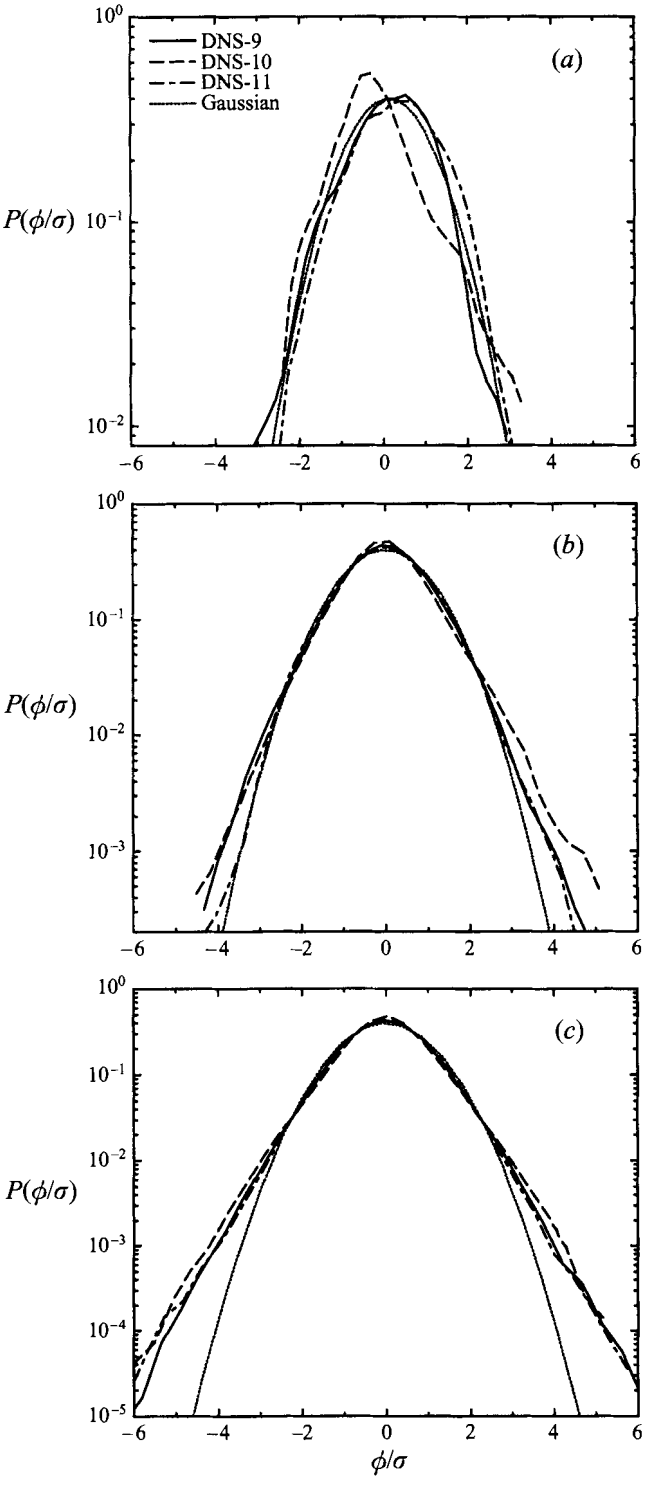

FIGURE 19. Normalized p.d.f.s of the bandpass-filtered scalar generated by DNS-9, DNS-10, and DNS-11 at $t_D = 4.286$. (*a*) LS: $0 < K \leqslant 3$, (*b*) IMS: $3 < K \leqslant 15$, (*c*) SS: $15 < K \leqslant 30$.

To show this, the time for DNS-12 is normalized by an 'effective' eddy turnover time which is the average of this time during the simulation after forcing is removed. The kurtosis results with the time axis scaled in this way are identified by DNS-12N in figure 18. Within the time duration of the simulation, the trend in kurtosis values in DNS-12N is close to that in DNS-10. However, the values are not identical. This is expected as the average of the eddy turnover time, as evaluated here, is not capable of reflecting the effects of the modified advection field. Nevertheless, all these results confirm that exponential p.d.f.s can be developed by adding an appropriate amount of large scales to the initial scalar field. It must be pointed out that the departure from Gaussian is not the explicit character of large scales. In figure 19 the p.d.f.s of filtered data are presented for cases DNS-9–DNS-11. Figure 19(*a*) indicates that the large scales, although somewhat asymmetric, are close to Gaussian. The IMS statistics, figure 19(*b*), do show long-tailed p.d.f.s with a small degree of asymmetry due to the distribution of the initial energy. The p.d.f.s for the scalar field in SS are similar and exponential in all the cases (figure 19*c*).

The variations of the kurtosis and the skewness values for DNS-13 are compared with those of DNS-11 in figure 20(*a*). In DNS-13 the initial scalar field, similar to DNS-11, is composed of a double-delta p.d.f. with significant energy at large scales. The results indicate that until $t_D \approx 12$, the statistics remain Gaussian in both cases. After this time, the kurtosis rises sharply in the case without a mean gradient (DNS-11), but there are no significant changes in the case with a mean gradient (DNS-13). The non-Gaussian behaviour in DNS-11 is the consequence of the presence of large initial scalar scales. It must be noted that this presence also results in skewed p.d.f.s in the simulations with a limited number of low-wavenumber modes. For the cases considered here, this is shown in figure 20(*a*) which in fact suggests large skewness values for DNS-11. Of course, if the calculations are repeated several times and statistics are gathered with a large number of realizations, the skewness would vanish but the kurtosis would not. However, the large scales do not cause skewed IMS p.d.f.s even those with flat-tail p.d.f.s., This is observed in figure 20(*b*) which shows that in DNS-11 and DNS-13 the p.d.f.s are fairly symmetric. Also, it is important to indicate that the behaviour shown in figure 20(*a*) for DNS-11 is not due to a numerical resolution problem. The normalized spectral density functions of the scalar (E_ϕ) and its dissipation (D_ϕ), shown in figure 20(*c*), are very similar in the two cases and are also similar to the corresponding spectra of the velocity field. The behaviour portrayed by DNS-11 and DNS-13 are also observed in two additional simulations (not shown here) in which the initial spectral density function obeys a power law of the form k^{-3}. For the case with $\mathscr{A} = 0$, the behaviour is similar to that in DNS-11, but with a negative skewness at long times. The results for $\mathscr{A} = 0.2$ are identical to those in DNS-13. All these results indicate that the presence of large scales is a strong source of non-Gaussian behaviour. This observation is very useful in interpreting some of the experimental results as discussed in the next section.

The non-Gaussian behaviour just described is not observed in the presence of a mean scalar gradient with the Scheme 2 initialization. The reason is that with such a

FIGURE 20. (*a*) Temporal variation of the DNS-generated scalar skewness and kurtosis. (*b*) p.d.f.s of the IMS ($3 < K \leqslant 15$) bandpass-filtered scalar at $t_D = 15.92$. (*c*) The spectral density functions at $t_D = 15.92$ of the velocity field $E_v(K)$, the scalar field $E_\phi(K)$, the dissipation of the velocity field $D_v(K)$ and the dissipation spectra of the scalar field $D_\phi(K)$. Forced turbulence, $Re_\lambda = 58$. The scalar field is initialized via Scheme 2 with an initial double-delta p.d.f. and with a double-hat spectrum, $K_{s1} = 1$, $K_{s2} = 8$, $\alpha = 1$. DNS-11 ($\mathscr{A} = 0$), DNS-13 ($\mathscr{A} = 0.2$).

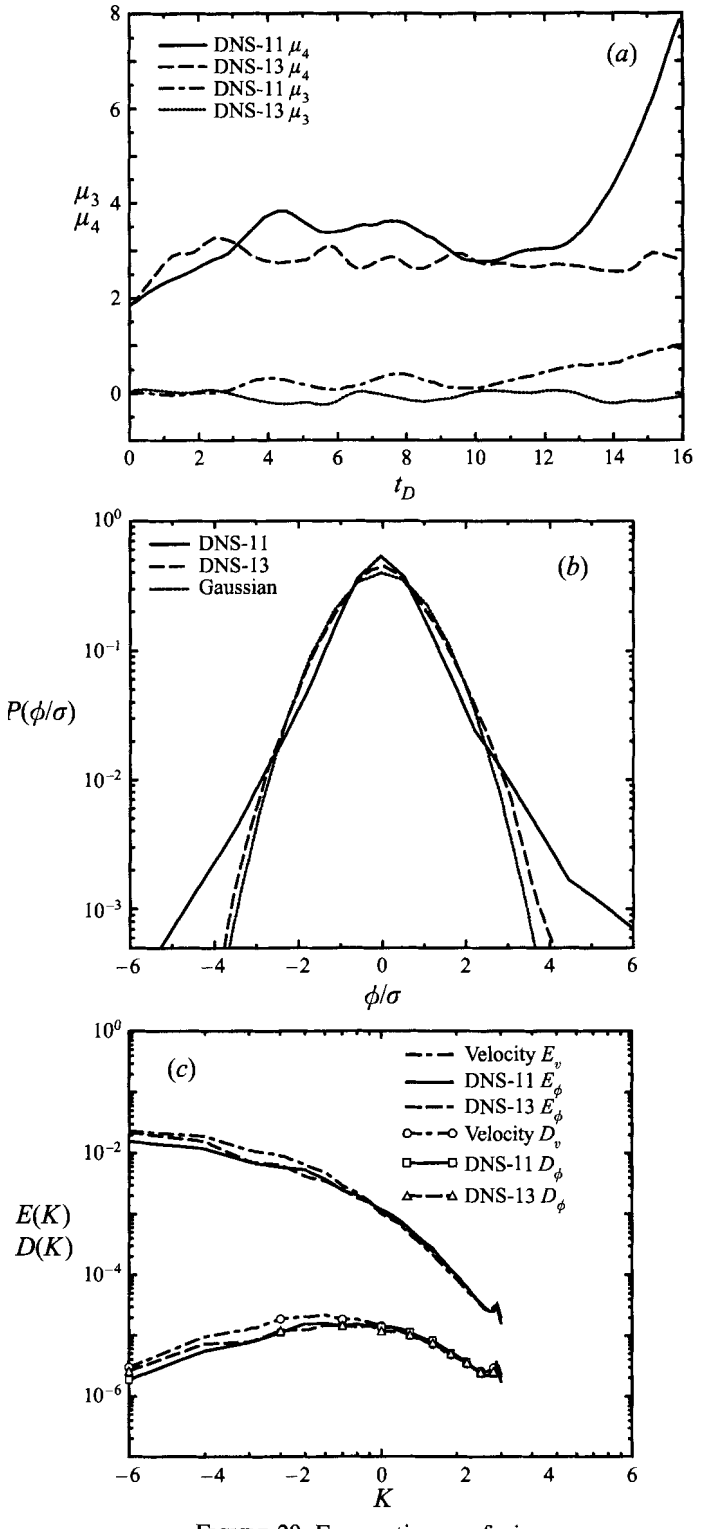

FIGURE 20. For caption see facing page.

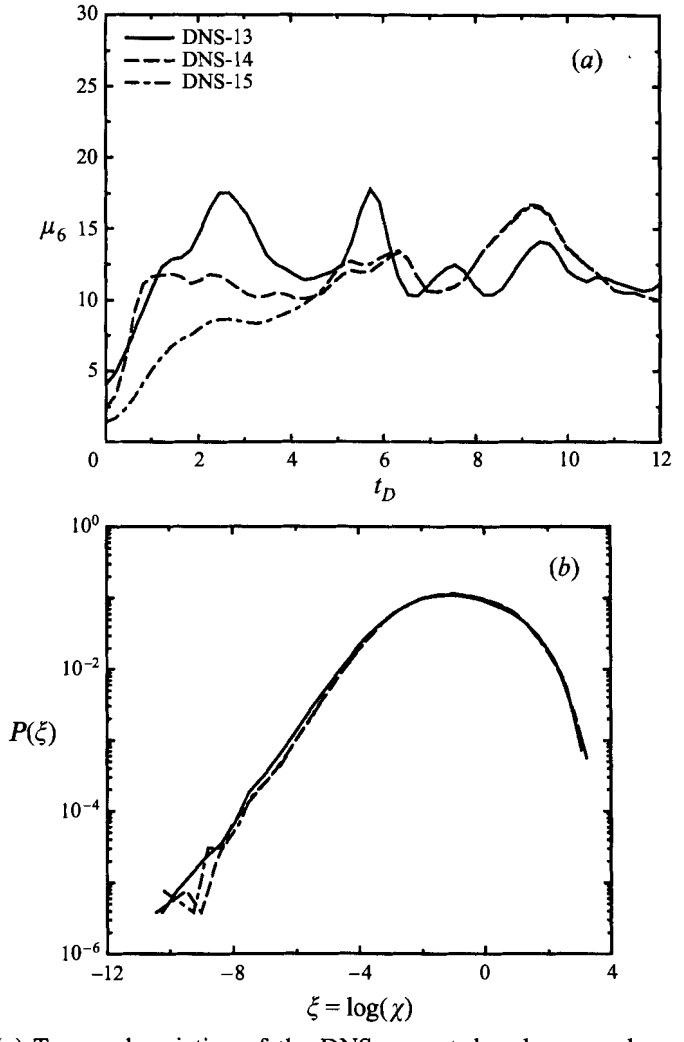

FIGURE 21. (*a*) Temporal variation of the DNS-generated scalar superskewness. (*b*) p.d.f.s of the scalar dissipation at $t_D = 12$. Forced turbulence, $Re_\lambda = 58$. The scalar field is initialized via Scheme 2 with an initial double-delta p.d.f. DNS-13 (double-hat spectrum, $K_{s1} = 1$, $K_{s2} = 8$, $\alpha = 1$, $\mathscr{A} = 0.2$), DNS-14 (top-hat spectrum, $K_s = 8, \mathscr{A} = 0.5$), DNS-15 (top-hat spectrum, $K_s = 1, \mathscr{A} = 0.5$).

gradient, the long-time statistics are fairly independent of initial conditions and also independent of the amplitude of the scalar gradient. This is demonstrated by the results for DNS-13–DNS-15 in which both the initial scalar conditions and the magnitude of $\mathscr{A}$ are varied. The results are given in figure 21(*a*) for the superskewness evolution and in figure 21(*b*) for the p.d.f.s of the scalar dissipation (χ) at $t_D = 12$. These figures demonstrate that the behaviour at long times is similar in all these cases (the spectral density functions are also similar, but are not shown). Of course, the independence from the initial conditions would be less pronounced in a decaying turbulence field.

In comparing the results generated by DNS with those via LEM one should keep in mind that the ratio of the length scale of the velocity to that of the scalar is an important parameter in the characterization of mixing. In DNS, these scales are limited by the computational domain (box size) at the upper bound. The same is also true in LEM but the scales can be imposed more independently of each other

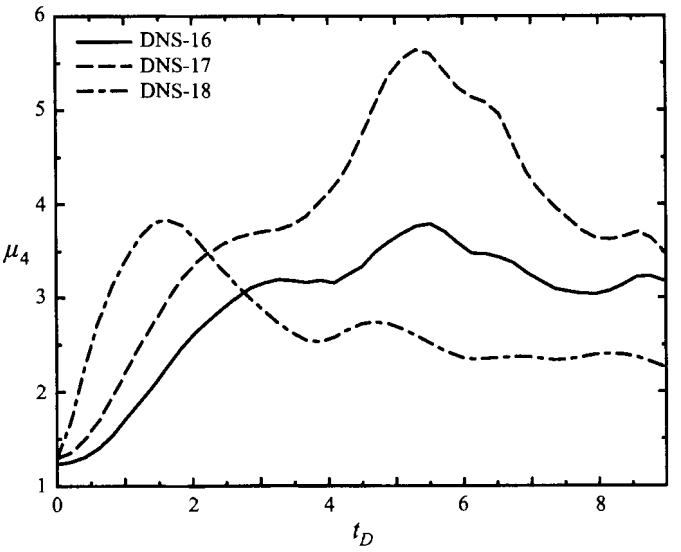

FIGURE 22. Temporal variation of the DNS-generated scalar kurtosis. Forced turbulence, $Re_\lambda = 58$. The scalar field is initialized via Scheme 3. DNS-16 (square wave, $Sc = 0.5$), DNS-17 (double square wave, $Sc = 0.5$), DNS-18 (double square wave, $Sc = 0.05$).

and with a higher degree of freedom in specifying the ranges. Here, it is shown that with the initialization of the scalar field in the form of square waves, trends similar to those depicted by LEM are observed. The simulations for $Sc = 0.5$ are labelled DNS-16 and DNS-17. For the former, a single square scalar wave (in the y-direction) is imposed. For the latter, a double square wave is imposed. Note that while the initial scalar profile in the y-direction is similar to that in the LEM initialization (figure 1), the initial scalar fields are not identical owing to the three-dimensionality of the DNS. The results in figure 22 show that after an initial transient time, the kurtosis remains close to 3 in DNS-16. But it increases in DNS-17 with a higher rate toward a larger value before decreasing to the near-Gaussian value at long times. This behaviour is similar to that observed in LEM-3; however, here the departure from Gaussian is not very significant since the dominant scale of the velocity is of the same order as that of the scalar (LEM-6).

The influence of the Schmidt number on the scalar p.d.f. is difficult to determine by DNS, as only a limited range of this parameter can be considered by direct simulations. However, some features are captured by a limited number of simulations and are discussed here. In DNS-18, the same initialization as DNS-17 is employed but with $Sc = 0.05$. The results in figure 22 indicate that by decreasing Sc the kurtosis grows faster initially, but then decreases and relaxes to a value less than 3. In these cases, the dominant scale of the velocity is of the same magnitude as that of the scalar. Thus the effect of Sc should be, and is, the same as that presented in figure 8 showing the difference between cases LEM-6 and LEM-22. Further extensive simulations with broader ranges of the length scales and the Schmidt number are required to generalize the influence of Sc on the scalar p.d.f. which (as shown in both the LEM and the DNS results) can be very complex. However, it seems that the effect of Sc on the scalar spatial-derivatives is somewhat less complex. In all the cases considered here it was observed that as Sc decreases, the intermittency of the scalar derivatives is less pronounced. This observation is consistent with previously established results (Kerr 1985).

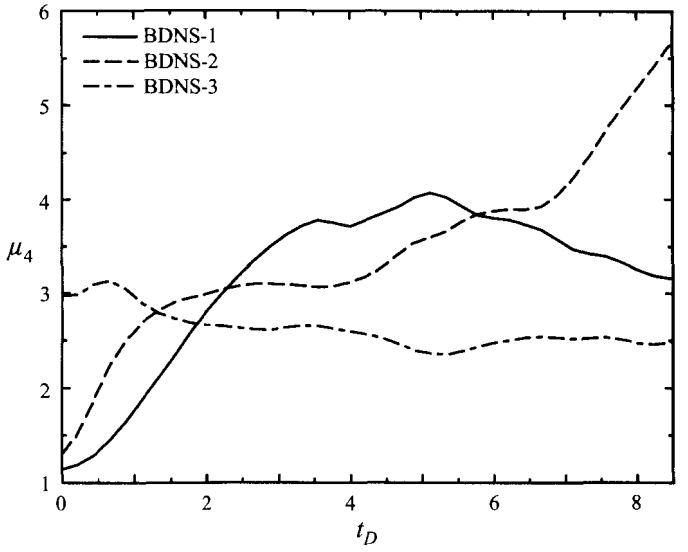

FIGURE 23. Temporal variation of the DNS-generated scalar kurtosis. Forced turbulence, $Re_\lambda = 80$. BDNS-1 (Scheme 3: double square wave, $\mathscr{A} = 0$), BDNS-2 (Scheme 2: double-hat spectrum, $K_{s1} = 1$, $K_{s2} = 8$, $\alpha = 0.125$, $\mathscr{A} = 0$), BDNS-3 (Scheme 1: Gaussian, $K_s = 8$, $\mathscr{A} = 0.5$).

An important characteristic displayed in DNS results is the lack of an exponential p.d.f. in all the simulations with an imposed mean scalar gradient. This is consistent with the analysis of Kimura & Kraichnan (1993), but is not in accord with that suggested by Pumir *et al.* (1991), Jayesh & Warhaft (1992) and Holzer & Siggia (1994). To confirm this finding, and also to study mixing at larger Reynolds numbers here a few additional simulations are performed with a higher resolution (128^3 collocation points). The conditions for these simulations are listed in table 3. Cases BDNS-1, BDNS-2, and BDNS-3 are initialized in a manner similar to DNS-17, DNS-10 and DNS-1(IV), respectively, but with a larger magnitude of the Reynolds number. Figure 23 indicates that the behaviour of BDNS-1 is similar to that of DNS-17, but with less deviation from Gaussian at long times. This is expected since in these two cases (DNS-17, BDNS-1) the largest scales of the scalar and the velocity fields are nearly equal and the initial scalar field is composed of two large slabs. The increase in *Re* provides a better stirring of the unmixed initial scalar field. Thus the p.d.f. at long times would be closer to Gaussian. The evolution of the kurtosis for BDNS-2 does not exhibit the same trend since the long-time p.d.f. is exponential. In this case, the separation of initial scalar length scales is more clearly established and the large scales have a smaller weight. As indicated before, the presence of rare large scales (small α values) in the initial field is sufficient to cause non-Gaussian behaviour as shown here by large values of the kurtosis in BDNS-2. The results in BDNS-3 are nearly identical to those in DNS-1(IV, V) in which the kurtosis values remain near 3. This indicates that in the presence of a constant mean gradient, the p.d.f. remains close to Gaussian regardless of the value of the Reynolds number. It is useful to note that the magnitude of the Reynolds number based on the integral length scale (Re_l) here is twice the critical *Re* above which Jayesh & Warhaft (1992) suggest exponential p.d.f.s should prevail.

Finally, some of the present results are compared with available experimental data. A quantitative comparison is made here; further qualitative comparisons are made

Variable	DNS-3(IV)	TW94	TV92	BTC85
$\left\langle \left(\frac{\partial\phi}{\partial x}\right)^3 \right\rangle \Big/ \left\langle \left(\frac{\partial\phi}{\partial x}\right)^2 \right\rangle^{3/2}$	−0.09	<0.1	small	small
$\left\langle \left(\frac{\partial\phi}{\partial y}\right)^3 \right\rangle \Big/ \left\langle \left(\frac{\partial\phi}{\partial y}\right)^2 \right\rangle^{3/2}$	1.67	1.8	1.2	1.4
$\left\langle \left(\frac{\partial\phi}{\partial x}\right)^4 \right\rangle \Big/ \left\langle \left(\frac{\partial\phi}{\partial x}\right)^2 \right\rangle^{2}$	7.32	8.5	–	–
$\left\langle \left(\frac{\partial\phi}{\partial y}\right)^4 \right\rangle \Big/ \left\langle \left(\frac{\partial\phi}{\partial y}\right)^2 \right\rangle^{2}$	9.21	10.0	–	–
$\langle u\phi\rangle/(\langle\phi^2\rangle\langle u^2\rangle)^{1/2}$	−0.009	small	small	small
$\langle v\phi\rangle/(\langle\phi^2\rangle\langle v^2\rangle)^{1/2}$	−0.586	−0.7	−0.68	−0.65
$\langle(u\phi)^3\rangle/(\langle\phi^2\rangle\langle u^2\rangle)^{3/2}$	−0.101	–	–	–
$\langle(v\phi)^3\rangle/(\langle\phi^2\rangle\langle v^2\rangle)^{3/2}$	−2.398	–	−2.1	–
$\langle(u\phi)^4\rangle/(\langle\phi^2\rangle\langle u^2\rangle)^{2}$	6.583	–	–	–
$\langle(v\phi)^4\rangle/(\langle\phi^2\rangle\langle v^2\rangle)^{2}$	11.61	–	11.0	–

TABLE 4. Comparison between the present simulated results and experimental measurements for some of the variables for cases with a constant mean scalar gradient. In the experiments, $Re_\lambda \approx 40$. TW94, TVA92 and BTC85 correspond to Tong & Warhaft (1994), Thoroddsen & Van Atta (1992) and Budwig *et al.* (1985), respectively.

in the next section. The experimental data considered are those provided by Budwig *et al.* (1985), Thoroddsen & Van Atta (1992) and Tong & Warhaft (1994). It must be indicated, however, that not all the conditions and the measured results are identical in these experiments. Moreover, some of the measured statistics are not invariable in each experiment and they are subject to change depending on the location of the measurements. In analysing the simulated results using such experiments, at least in the context considered here, it is more appropriate to make qualitative comparisons as done in the next section. Nevertheless, it is useful to examine the trends established numerically in the light of the laboratory data.

All our results indicate that intermittency of the scalar derivative in the x-direction (perpendicular to the direction of the mean scalar gradient) is enhanced as the Reynolds number increases. The same is true for the derivative in the y-direction (parallel to the mean gradient direction), but with higher skewness magnitudes. At the range considered the skewness does not seem to be noticeably dependent on Re. These results are consistent with recent results based on the experiments of Tong & Warhaft (1994) and the numerical results of Pumir (1994). Also, the simulated p.d.f.s of the velocity-scalar fluctuations ($u\phi$ and $v\phi$) are exponential with relatively high skewness values for $v\phi$. This is in accord with the experiments of Thoroddsen & Van Atta (1992). Table 4 provides a quantitative comparison between all the simulated and laboratory results. For this comparison, DNS-3(IV) is considered since in this case a mean scalar gradient is imposed in accord with the experiments, and the Reynolds number is close to that in the experiments of Thoroddsen & Van Atta (1992) and Tong & Warhaft (1994). The statistics in this table are generated via time averaging over several realizations, in addition to space averaging. This is justifiable since in the

presence of the mean scalar gradient, the field can be assumed quasi-stationary (or in a sense ergodic) at long times.

In accord with the experimental measurements, the numerical results show negligible skewness values for the scalar derivative and the scalar flux in the x-direction, but indicate significant skewness values for the y-derivative and the scalar flux in the y-direction. The simulated skewness and kurtosis values of the scalar gradients are close to those in the experiments of Tong & Warhaft (1994). With inclusion of data for BDNS-3 (with $Re_\lambda = 80$) for the y-derivative skewness (1.59) and kurtosis (10.82), the numerical results indicate a relative independence of the skewness and Re_λ, and a scaling of $Re^{0.21}$ for the kurtosis. These scalings are in accord with those suggested by Tong & Warhaft (1994). The experimental values for the mean flux $\langle v\phi \rangle$ are underestimated by DNS, but the simulated values of the skewness and the kurtosis of this flux compare well with the measurements (Thoroddsen & Van Atta 1992).

4. Further discussion

In the light of the numerical results generated, here an interpretation is provided of some of the features observed in recent laboratory and numerical experiments on scalar mixing in turbulent flows.

In the mixing experiments of Gollub *et al.* (1991) and Lane *et al.* (1993) of a flow between heated walls, the transition from a Gaussian to an exponential scalar p.d.f. is accompanied by a sharp increase in the effective diffusivity and a decrease in the magnitude of the mean scalar gradient within a region far from the boundary layers. Most of the temperature drop occurs in the boundary layer, and the interior mean temperature varies linearly from one side to the other. However, the magnitude of the mean temperature gradient in the interior regions varies nonlinearly with the Reynolds number. The steep decline of the magnitude of the mean gradient near the critical Re implies a substantial increase in the bulk thermal transport over a relatively narrow region near the wall. The sharp growth of the skewness of scalar fluctuations for Reynolds numbers greater than a critical value is also an important characteristic of this experiment. This skewness is preserved even when considering a large sample size and is not a consequence of limited statistical data or measurement errors. Lane *et al.* (1993) explain that the skewness may be generated by a weak large-scale flow drift which might be caused by flow instabilities at high Re. They also indicate that by increasing the correlation length scale of the velocity from 0.48 to 1.7 cm the scalar p.d.f. remains Gaussian even up to $Re = 8000$. The critical Re above which sudden changes occur in the bulk properties in this case is 1000. In several aspects, these results are in accord with our findings. Before the transition Re the statistics are mostly determined by the mean gradient. The unmixed large-scale plumes within the boundary layer are stable and do not mix with interior fluids. This means that the statistics are dictated by the interior linear (approximately) mean scalar profile where the fluids are well mixed. Therefore, the p.d.f. remains approximately Gaussian. As Re increases to its critical value, the large scales at the boundary become unstable and are engulfed within the interior regions of the flow. These are still large-scale structures and their combination with the mixed interior fluid results in skewed p.d.f.s with broad tails. This behaviour is observed in our LEM (cases LEM-3, LEM-8, LEM-14) and DNS (cases DNS-10, DNS-11, BDNS-2) results. The instability of large scales facilitates the transport of the energy-containing scales at the boundary into the interior region, resulting in the increase of the heat flux and the effective diffusivity. At the same time, the fluid within the interior region

is more vigorously mixed yielding a low value of the local mean scalar gradient. The fluid in this region is continuously fed by rare large scales, and the unmixed thermal plumes are convected from boundary flows and are stirred by the interior flow. If the feeding by the large scales is continuous, as it is in the experiments, the p.d.f. remains exponential. If there is no influx of large scales, then mixing is transient and a Gaussian p.d.f. is eventually observed. These observations are in accord with our simulations as we show that the presence of rare large scales yields exponential p.d.f.s. However, a linear mean scalar profile is not responsible for this behaviour as in all our simulations pertaining to this issue the magnitude of the mean gradient is zero. Note that the significant portion of the temperature difference occurs near the walls and a substantial amount of heat transfer is due to the bulk motion of the fluid. One cannot expect to have significant 'unmixed' regions with exponential p.d.f.s, and at the same time expect an increase in the heat transfer and the thermal diffusivity. Therefore, it may not necessarily be the mean scalar gradient that is causing non-Gaussian intermittency, but it is the bulk fluid motion which introduces the large-scale boundary fluids into the central region. Of course the quantitative outcome depends on the magnitudes of the length scales, Re and Sc, and also the geometry of the flow configuration.

In the experiments of Gollub *et al.* (1991) and Lane *et al.* (1993) it is also shown that weak large scales can cause skewed p.d.f.s, the degree of which is enhanced as Re increases. This behaviour is more pronounced when the largest length scale of the velocity is smaller than that of the scalar, and disappears when the velocity length scale increases. Moreover, with an increase of the velocity scale from a size smaller than the scalar scale to one larger, the p.d.f. changes from exponential to Gaussian. It has been suggested (Lane *et al.* 1993; Kimura & Kraichnan 1993) that this behaviour could be due to non-isotropy or non-homogeneity of the velocity field. This does not seem to be the case as the results of previous laboratory (Tavoularis & Corrsin 1981*a*) and numerical (Rogers, Moin & Reynolds 1986; Miller *et al.* 1995) experiments on non-isotropic shear flows show Gaussian scalar p.d.f.s even at large Reynolds numbers. In fact, the non-homogeneity in the experiments of Lane *et al.* (1993) is more significant when Re is less than the critical value, i.e. when the p.d.f. is Gaussian. In DNS-11 we show that by an increase of the initial scalar energy at low wavenumbers, the presence of large scales causes skewed p.d.f.s. But this is not due to the presence of the mean scalar gradient. This skewness is expected to vanish if a large number of realizations are considered.

Notwithstanding the 'active' role of scalars, the behaviour discussed above is also observed in the convection experiments. In the Rayleigh–Bérnard experiments of Solomon & Gollub (1991), the temperature p.d.f. is Gaussian or exponential if the Rayleigh number is below or above the transition value (Ra_t). For $Ra < Ra_t$, the presence of thermal plumes is detected. These plumes remain attached to the wall from which they erupt, but span the layer all the way to the opposite wall without breaking. In the more energetic state, when $Ra > Ra_t$ the plumes are broken apart by turbulence resulting in a flow dominated by disconnected and freely convecting fluid blobs (thermals). In the 'soft turbulence' regime ($Ra < Ra_t$), the influence of thermal plumes on the temperature p.d.f. is negligible. They only contribute to the mean transport across the cell and do not significantly affect the temperature fluctuations. In the hard turbulence regime ($Ra > Ra_t$), the breaking of large scales contributes to the scalar fluctuations throughout the cell including the central mixing core. In this regime, Zocchi, Moses & Libchaber (1991) indicate that most of the temperature drop occurs near the boundary plates and the bulk of the interior fluid is at constant

temperature. The experiments of the Chicago group indicate a Gaussian p.d.f. in the soft turbulence regime and an exponential p.d.f. in the hard turbulence regime. Our results, however, imply that it is not only the magnitude of Ra_t that determines the p.d.f.; the influence of the thermal plumes is also important and should be considered. In other words, hard–soft turbulence regions may not necessarily be associated with exponential–Gaussian p.d.f.s. Rather, it is the distribution of the scalar length scales and their relation to the velocity length scales that are important in determining the p.d.f.. Note that the size of the plumes and their eruption are controlled by the aspect ratio of the cell and the magnitude of Ra. As the plumes grow and break, they interact with the fluid within the core. In the core, therefore, the p.d.f. is governed by a weighted sum of the statistics of the incoming unmixed flow with that of the well-mixed original core fluid. As we show in DNS-10 and BDNS-2 this can cause non-Gaussian behaviour in accord with that observed experimentally. In this regard, our results are consistent with those obtained by Christie & Domaradzki (1993, 1994) as they indicate that at a fixed Ra, both Gaussian and exponential p.d.f.s can be generated by varying the cell aspect ratio. Our arguments are also in accord with Solomon & Gollub (1991) who indicate that the scalar p.d.f. is chiefly controlled by the coherency of thermal plumes.

The stratified thermal convection experiments of Thoroddsen & Van Atta (1992) provide further evidence in support of our physical arguments. The inherent stability of the flow in this low-Re experiment is sufficient to keep the p.d.f. Gaussian, even with an imposed mean scalar gradient. Gaussian p.d.f.s are observed in all the cases considered in this experiment, consistent with all the results portrayed here for DNS-1(IV), DNS-13, BDNS-3. Further experiments at large Reynolds numbers would be very valuable in generalizing the conclusions drawn from these simulations.

The experimental results of Jayesh & Warhaft (1992) on passive scalar mixing in decaying grid-generated turbulence indicate the presence of both Gaussian and exponential scalar p.d.f.s. They suggest that in the presence of a constant mean scalar gradient, after a complex initial evolution the p.d.f. adopts an exponential form if the Reynolds number based on the integral flow scale (Re_l) is larger than a critical value ($Re_c \approx 70$). In the absence of the mean gradient, the p.d.f. is skewed but approximately Gaussian. The results of earlier experiments of Tavoularis & Corrsin (1981*a*) in turbulent shear flows with a constant mean scalar gradient suggest Gaussian p.d.f.s even for Reynolds numbers much larger than Re_c of Jayesh & Warhaft (1992). It seems unlikely that the non-isotropic nature of shear turbulence is responsible for the deviation from Gaussian as witnessed in the experiments of Lane *et al.* (1993) and the convection experiments of Heslot *et al.* (1987). In all the cases considered in our DNS of flows with a constant mean gradient, the p.d.f. is Gaussian regardless of the initial conditions and the magnitude of the Reynolds number. This is consistent with the experimental findings of Tavoularis & Corrsin (1981*a*), DNS results of Rogers, Mansour & Reynolds (1989) and recent analyses of Kimura & Kraichnan (1993), but not in accord with the numerical results of Holzer & Siggia (1994). We also show that once non-Gaussian statistics are formed they tend to exist longer in a decaying turbulent flow than in a forced stationary flow. This is especially true when there are large-scale scalar fluctuations that cannot be stirred by small-velocity eddies, even in the presence of a constant mean gradient. It appears that this condition is present in the experiments of Jayesh & Warhaft (1992).

One notable difference between the experiments of Jayesh & Warhaft (1992) and Tavoularis & Corrsin (1981*a*) is the ratio of the length scales of the scalar to the velocity. In Jayesh & Warhaft (1992) for the case with a mean gradient this

ratio is greater than unity, but in Tavoularis & Corrsin (1981*a*) it is smaller than unity. Thus our results in the cases with a mean scalar gradient are expected to be consistent with those of Tavoularis & Corrsin (1981*b*). The analysis of Kimura & Kraichnan (1993) shows that a nonlinear or a piecewise linear mean scalar profile can cause significant non-Gaussian behaviour. In our DNS, a perfectly linear mean scalar profile for the whole domain is imposed; therefore, the length scales of scalar fluctuations are determined by the forcing function due to the mean gradient in (9). This does not appear to be the case in the experiments since the mean scalar profile, even if perfectly linear, does not extend over the entire domain. Thus it is possible that the effect of initial (inlet) conditions are preserved in governing the consequent statistics. Furthermore, in the presence of the mean gradient in Jayesh & Warhaft's (1992) experiments, the large scalar scales evaluated based on the peak of the scalar spectrum (l_θ) remain larger than the velocity integral scale along the tunnel. From the measured temperature spectrum it can be deduced that scalar scales up to 70 times larger than l_θ are present. For example, it is shown that scalar scales larger than $7l_\theta$ contribute to 8% of the total scalar variance. In our simulations we show that this amount of large scales is sufficient to create significant departure from Gaussian especially when $l_u < l_\theta$. Despite their contribution in developing exponential-tail p.d.f.s, these large scales do not necessarily portray non-Gaussian behaviour themselves. In fact, if these scales are filtered out, the p.d.f. of the retained field exhibits a strong exponential behaviour. This is observed in our results presented in figure 19(*b*).

In the absence of the mean gradient, the reported results in Jayesh & Warhaft (1992) correspond to the case where the scalar length scale is smaller than that of the velocity. For this case, based on our LEM (cases LEM-6, LEM-10, LEM-16) and DNS (cases DNS-5, DNS-16) results, we expect the scalar p.d.f. to be near Gaussian. As indicated by Warhaft & Lumley (1978) in grid-generated turbulence experiments it is not clear how to change the thermal length scales (by grid heating) without affecting the velocity field. This is an important issue awaiting further investigations, especially by laboratory experiments.

5. Concluding remarks

The results of our numerical experiments reveal the intricate physics of scalar mixing and the complex role played by the combined influences of advection and molecular diffusion in turbulent flows. The primary observation made here is to verify that the long-time p.d.f. of a passive scalar in homogeneous turbulent flows is not necessarily Gaussian (or of any other particular form), and the fate of mixing is dependent on several factors. The objective of this work is to identify some of the causes for non-Gaussian behaviour of the scalar field and to determine the influence of several flow parameters in governing the scalar statistics. Aided by the analyses of the numerically generated data, an attempt is made to interpret the results provided in several recent laboratory experiments. With this interpretation, it is easy to see that there are many more possibilities (than those discussed here) for generating non-Gaussian p.d.f.s. However, there are several conclusions that can be drawn from the simulated results. These conclusions are itemized here, with the caveat that they are established in the range of parameters, resolution, and within the time durations considered in the present simulations:

(i) Two mechanisms are identified for causing exponential p.d.f.s of the scalar amplitude due to the concurrent actions of advection and diffusion. (1) A non-uniform

action of advection on the large and the small scalar scales: for this, the dominant scale of advection should be smaller than that of the scalar and the weight of the large scalar scales should be 'appropriately' imposed. By 'appropriate' it is meant that there is some energy at large scalar scales, but its magnitude is smaller than that at other scales. (2) The nonlinear interaction of the scalar and the velocity fluctuations at small scales: in this case, the scalar tends to be correlated with the scalar gradient due to the smoothing effect of molecular diffusion on the scalar gradient. This correlation leads to a weak non-Gaussian behaviour and can be enhanced by increasing the weight of small scalar scales.

(ii) Although the presence of an appropriate amount of large scalar scales is a source of non-Gaussian behaviour, the p.d.f.s of the large scales themselves are not necessarily exponential.

(iii) In the absence of a mean scalar gradient, i.e. a decaying scalar field, the p.d.f. is very sensitive to the initial conditions. In the presence of this gradient, non-Gaussian behaviour is not sustained regardless of initial conditions.

(iv) The statistical behaviour is different in a stationary turbulence field from that in a decaying field. Once non-Gaussian behaviour is developed, it has a tendency to survive for a longer time in a decaying field.

(v) Contrary to its role in the scalar-derivative p.d.f.s, the Schmidt number exhibits a rather complex influence on the p.d.f.s of the scalar amplitude. In most of the cases considered, non-Gaussian behaviour becomes more pronounced as the magnitude of the Schmidt number is increased. However, an opposite behaviour can be observed under the first criterion (noted above). Further laboratory and numerical experiments with large Sc values are required to investigate this issue.

(vi) It is suggested that the non-Gaussian behaviour observed in recent laboratory experiments on passive scalar mixing may not be necessarily due to the presence of a linear mean scalar profile. It is argued that the initial/boundary conditions, and/or the nonlinearity of the mean scalar profile could be the cause of this behaviour.

(vii) It is suggested that the non-Gaussian behaviour observed in recent convection laboratory experiments may not be necessarily due the presence of a hard-turbulence regime. It is the dynamics of the thermal plumes that could be the cause.

(viii) The simulated results pertaining to small-scale intermittency are in accord with laboratory experimental results. The DNS generated statistics of the scalar derivatives and the velocity-scalar fluctuations are also in agreement with laboratory measurements.

A challenging next step would be the analysis of mixing for active scalars and/or chemically reactive flows (Libby & Williams 1994) in both homogeneous and non-homogeneous flows.

We are grateful to Drs Alan Kerstein and Patrick McMurtry for many helpful discussions. This work is sponsored by the Office of Naval Research under Grant N00014-94-1-0667 and by the National Science Foundation under Grant CTS-9253488. Computational resources are provided by the SEAS Computing Center at SUNY-Buffalo and by the NCSA at the University of Illinois at Urbana.

REFERENCES

ANDREWS, L. C. & SHIVAMOGGI, B. K. 1990 The gamma distribution as a model for temperature dissipation in intermittent turbulence. *Phys. Fluids* A **2**, 105–110.

ANSELMET, F., GAGNE, Y., HOPFINGER, E. J. & ANTONIA, R. A. 1984 High-order velocity structure functions in turbulent shear flows. *J. Fluid Mech.* **140**, 63–89.

ANTONIA, R. A., HOPFINGER, E. J., GAGNE, Y. & ANSELMET, F. 1984 Temperature structure functions in turbulent shear flows. *Phys. Rev.* A **30**, 2704–2707.

ANTONIA, R. A. & VAN ATTA, C. W. 1978 Structure functions of temperature fluctuations in turbulent shear flows. *J. Fluid Mech.* **84**, 561–580.

ASHURST, W. T., CHEN, J.-Y. & ROGERS, M. M. 1987*a* Pressure gradient alignment with strain rate and scalar gradient in simulated Navier-Stokes turbulence. *Phys. Fluids* **30**, 3293–3294.

ASHURST, W. T., KERSTEIN, A. R., KERR, R. M. & GIBSON, C. H. 1987*b* Alignment of vorticity and scalar gradient with strain rate in simulated Navier-Stokes turbulence. *Phys. Fluids* **30**, 2343–2353.

BATCHELOR, G. K. & TOWNSEND, A. A. 1949 The nature of turbulence motion at large wave numbers. *Proc. R. Soc. Lond.* A **199**, 534–550.

BELMONTE, A., TILGNER, A. & LIBCHABER, A. 1994 Temperature and velocity boundary layers in turbulent convection. *Phys. Rev.* E **50**, 269–279.

BRODKEY, R. S. (ed.) 1975 *Turbulence in Mixing Operations.* Academic.

BUDWIG, R., TAVOULARIS, S. & CORRSIN, S. 1985 Temperature fluctuations and heat flux in grid-generated isotropic turbulence with streamwise and transverse mean-temperature gradients. *J. Fluid Mech.* **153**, 441–460.

CASTAING, B., GAGNE, Y. & HOPFINGER, E. J. 1990 Velocity probability density functions of high Reynolds number turbulence. *Physica* D **46**, 177–200.

CASTAING, B., GUNARATNE, G., HESLOT, F., KADANOFF, L., LIBCHABER, A., THOMAE, S., WU, X. Z., ZALESKI, S. & ZANETTI, G. 1989 Scaling of hard thermal turbulence in Rayleigh–Bernard convection. *J. Fluid Mech.* **204**, 1–30.

CHEN, H., CHEN, S. & KRAICHNAN, R. H. 1989 Probability distribution of a stochastically advected scalar field. *Phys. Rev. Lett.* **63**, 2657–2660.

CHEN, S., DOOLEN, G., HERRING, J. R., KRAICHNAN, R. H., ORSZAG, S. A. & SHE, Z. S. 1993 Far-dissipation range of turbulence. *Phys. Rev. Lett.* **70**, 3051–3054.

CHING, E. S. C. & TU, Y. 1994 Passive scalar fluctuations with and without a mean gradient: A numerical study. *Phys. Rev.* E **49**, 1278–1282.

CHRISTIE, S. L. & DOMARADZKI, J. A. 1993 Numerical evidence for the nonuniversality of the soft/hard turbulence classification for thermal convection. *Phys. Fluids* A **5**, 412–421.

CHRISTIE, S. L. & DOMARADZKI, J. A. 1994 Scale dependence of the statistical character of turbulent fluctuations in thermal convection. *Phys. Fluids* **6**, 1848–1855.

CURL, R. L. 1963 Dispersed phase mixing: I. Theory and effects in simple reactors. *AIChE J.* **9**, 175–181.

DOPAZO, C. 1994 Recent developments in p.d.f. methods. In *Turbulent Reacting Flows* (ed. P. A. Libby & F. A. Williams), pp. 375–474. Academic.

DOPAZO, C. & O'BRIEN, E. E. 1976 Statistical treatment of non-isothermal chemical reactions in turbulence. *Combust. Sci. Tech.* **13**, 99–112.

ESWARAN, V. & POPE, S. B. 1988 Direct numerical simulations of the turbulent mixing of a passive scalar. *Phys. Fluids* **31**, 506–520.

FRANKEL, S. H. 1993 Probabilistic and deterministic description of turbulent flows with nonpremixed reactants. PhD thesis, Department of Mechanical and Aerospace Engineering, State University of New York at Buffalo, Buffalo, NY.

FRANKEL, S. H., MADNIA, C. K. & GIVI, P. 1993 Comparative assessment of closures for turbulent reacting flows. *AIChE J.* **39**, 899–903.

GIVI, P. 1989 Model free simulations of turbulent reactive flows. *Prog. Energy Combust. Sci.* **15**, 1–107.

GIVI, P. 1994 Spectral and random vortex methods in turbulent reacting flows. In *Turbulent Reacting Flows* (ed. P. A. Libby & F. A. Williams), pp. 475–572. Academic.

GIVI, P. & MADNIA, C. K. 1993 Spectral methods in combustion. In *Numerical Modeling in Combustion* (ed. T. J. Chung), pp. 409–452. Taylor & Francis.

GIVI, P. & MCMURTRY, P. A. 1988 Non-premixed reaction in homogeneous turbulence: Direct numerical simulations. *AIChE J.* **34**, 1039–1042.

GOLLUB, J. P., CLARKE, J., GHARIB, M., LANE, B. & MESQUITA, O. N. 1991 Fluctuations and transport in a stirred fluid with a mean gradient. *Phys. Rev. Lett.* **67**, 3507–3510.

GURVICH, A. S. & YAGLOM, A. M. 1967 Breakdown of eddies and probability distributions for small-scale turbulence. *Phys. Fluids Suppl.* **10**, S59–S65.

HAWTHORNE, W. R., WEDELL, D. S. & HOTTEL, H. C. 1949 Mixing and combustion in turbulent gas jets. In *3rd Symp. on Combustion, Flames and Explosion Phenomena*, pp. 266–288. The Combustion Institute, Pittsburgh, PA.

HESLOT, F., CASTAING, B. & LIBCHABER, A. 1987 Transitions to turbulence in helium gas. *Phys. Rev.* A **36**, 5870–5873.

HILL, J. C. 1979 Simulation of chemical reaction in a turbulent flow. In *Proc. Second R. F. Ruth Chemical Engineering Research Symposium*, pp. 27–53. Ames, Iowa.

HOLZER, M. & PUMIR, A. 1993 Simple models of non-Gaussian statistics for a turbulently advected passive scalar. *Phys. Rev.* E **47**, 202–219.

HOLZER, M. & SIGGIA, E. D. 1994 Turbulent mixing of a passive scalar. *Phys. Fluids* **6**, 1820–1837.

HOSOKAWA, I. & YAMAMOTO, K. 1989 Fine structure of a directly simulated isotropic turbulence. *J. Phys. Soc. Japan* **58**, 20–23.

JABERI, F. A. & GIVI, P. 1995 Inter-layer diffusion model of scalar mixing in homogeneous turbulence. *Combust. Sci. Tech.* **104**, 249–272.

JABERI, F. A., MILLER, R. S. & GIVI, P. 1995 Conditional statistics in turbulent scalar mixing and reaction. *AIChE J.*, In press.

JANICKA, J., KOLBE, W. & KOLLMANN, W. 1979 Closure of the transport equation for the probability density function of turbulent scalar field. *J. Nonequil. Thermodyn.* **4**, 47–66.

JAYESH & WARHAFT, Z. 1991 Probability distribution of a passive scalar in grid-generated turbulence. *Phys. Rev. Lett.* **67**, 3503–3506.

JAYESH & WARHAFT, Z. 1992 Probability distribution, conditional dissipation, and transport of passive temperature fluctuations in grid-generated turbulence. *Phys. Fluids* A **4**, 2292–2307.

JIMENEZ, J., WRAY, A. A., SAFFMAN, P. G. & ROGALLO, R. S. 1993 The structure of intense vorticity in isotropic turbulence. *J. Fluid Mech.* **255**, 65–90.

KERR, R. M. 1983 High-order derivative correlations and the alignment of small-scale structures in isotropic numerical turbulence. *NASA TM* 84407.

KERR, R. M. 1985 High-order derivative correlations and the alignment of small-scale structures in isotropic numerical turbulence. *J. Fluid Mech.* **153**, 31–58.

KERR, R. M. 1990 Velocity, scalar and transfer spectra in numerical turbulence. *J. Fluid Mech.* **211**, 309–332.

KERSTEIN, A. R. 1988 A linear eddy model of turbulent scalar transport and mixing. *Combust. Sci. Tech.* **60**, 391–421.

KERSTEIN, A. R. 1989 Linear eddy modelling of turbulent transport. II: Applications to shear layer mixing. *Combust. Flame* **75**, 397–413.

KERSTEIN, A. R. 1990 Linear eddy modelling of turbulent transport. Part 3. Mixing and differential molecular diffusion in round jets. *J. Fluid. Mech.* **216**, 411–435.

KERSTEIN, A. R. 1991 Linear-eddy modelling of turbulent transport. Part 6. Microstructure of diffusive scalar mixing fields. *J. Fluid Mech.* **231**, 361–394.

KERSTEIN, A. R. 1992 Linear-eddy modelling of turbulent transport. Part 7. Finite-rate chemistry and multi-stream mixing. *J. Fluid Mech.* **240**, 289–313.

KERSTEIN, A. R. & MCMURTRY, P. A. 1994*a* Low wave number statistics of randomly advected passive scalars. *Phys. Rev.* E **50**, 2057–2063.

KERSTEIN, A. R. & MCMURTRY, P. A. 1994*b* Mean-field theories of random advection. *Phys. Rev.* E **49**, 474–482.

KIMURA, Y. & KRAICHNAN, R. H. 1993 Statistics of an advected passive scalar. *Phys. Fluids* A **5**, 2264–2277.

KOLMOGOROV, A. N. 1941 The local structure of turbulence in incompressible viscous fluid for large Reynolds numbers. *Dokl. Akad. Nauk SSSR* **30**, 301–305.

KOLMOGOROV, A. N. 1962 A refinement of previous hypotheses concerning the local structure of turbulence in a viscous incompressible fluid at high Reynolds number. *J. Fluid Mech.* **13**, 82–85.

KRAICHNAN, R. H. 1989 Closures for probability distributions. *Bull. Am. Phys. Soc.* **34**, 2298.

LANDAU, L. D. & LIFSHITZ, E. M. 1959 *Fluid Mechanics.* Pergamon.

LANE, B. R., MESQUITA, O. N., MEYERS, S. R. & GOLLUB, J. P. 1993 Probability distributions and thermal transport in a turbulent grid flow. *Phys. Fluids* A **5**, 2255–2263.

LEONARD, A. D. & HILL, J. C. 1988 Direct numerical simulation of turbulent flows with chemical reaction. *J. Sci. Comput.* **3**, 25–43.

LEONARD, A. D. & HILL, J. C. 1991 Scalar dissipation and mixing in turbulent reacting flows. *Phys. Fluids* A **3**, 1286–1299.

LEONARD, A. D. & HILL, J. C. 1992 Mixing and chemical reaction in sheared and nonsheared homogeneous turbulence. *Fluid Dyn. Res.* **10**, 273–297.

LIBBY, P. A. & WILLIAMS, F. A. (ed.) 1980 *Turbulent Reacting Flows.* Topics in Applied Physics, vol. 44. Springer.

LIBBY, P. A. & WILLIAMS, F. A. (ed.) 1994 *Turbulent Reacting Flows.* Academic.

MADNIA, C. K., FRANKEL, S. H. & GIVI, P. 1992 Reactant conversion in homogeneous turbulence: Mathematical modeling, computational validations and practical applications. *Theoret. Comput. Fluid Dyn.* **4**, 79–93.

MCMURTRY, P. A., GANSAUGE, T. C., KERSTEIN, A. R. & KRUEGER, S. K. 1993*a* Linear eddy simulations of mixing in a homogeneous turbulent flow. *Phys. Fluids* A **5**, 1023–1034.

MCMURTRY, P. A. & GIVI, P. 1989 Direct numerical simulations of mixing and reaction in a nonpremixed homogeneous turbulent flow. *Combust. Flame* **77**, 171–185.

MCMURTRY, P. A., MENON, S. & KERSTEIN, A. R. 1993*b* Linear eddy modeling of turbulent combustion. *Energy & Fuels* **7**, 817–826.

METAIS, O. & LESIEUR, M. 1992 Spectral large-eddy simulation of isotropic and stably stratified turbulence. *J. Fluid Mech.* **239**, 157–194.

MILLER, R. S. 1995 Passive scalar, magnetic field, and solid particle transport in homogeneous turbulence. PhD thesis, Department of Mechanical and Aerospace Engineering, State University of New York at Buffalo, Buffalo, NY.

MILLER, R. S., FRANKEL, S. H., MADNIA, C. K. & GIVI, P. 1993 Johnson-Edgeworth translation for probability modeling of binary scalar mixing in turbulent flows. *Combust. Sci. & Tech.* **91**, 21–52.

MILLER, R. S., JABERI, F. A., MADNIA, C. K. & GIVI, P. 1995 The structure and small-scale intermittency of passive scalars in homogeneous turbulence. *J. Sci. Comput.* **10**, 151–180.

MIYAWAKI, O., TSUJIKAWA, H. & URAGUCHI, Y. 1974 Turbulent mixing in multi-nozzle injector tubular mixers. *J. Chem. Engng Japan* **7**, 52–74.

MONIN, A. S. & YAGLOM, A. M. 1975 *Statistical Fluid Mechanics*, Vol. 2. MIT Press.

NOMURA, K. K. & ELGHOBASHI, S. E. 1992 Mixing characteristics of an inhomogeneous scalar in isotropic and homogeneous sheared turbulence. *Phys. Fluids* A **4**, 606–625.

O'BRIEN, E. E. 1980 The probability density function (p.d.f.) approach to reacting turbulent flows. In *Turbulent Reacting Flows* (ed. P. A. Libby & F. A. Williams), pp. 185–218. Springer.

OBUKHOV, A. M. 1962 Some specific features of atmospheric turbulence. *J. Fluid Mech.* **13**, 77–81.

POPE, S. B. 1979 The statistical theory of turbulent flames. *Phil. Trans. R Soc. Lond.* A **291**, 529–568.

POPE, S. B. 1982 An improved turbulent mixing model. *Combust. Sci. Tech.* **28**, 131–145.

POPE, S. B. 1985 p.d.f. methods for turbulent reactive flows. *Prog. Energy Combust. Sci.* **11**, 119–192.

POPE, S. B. 1990 Computations of turbulent combustion: Progress and challenges. In *Proc. 23rd Symp. (Intl) on Combustion*, pp. 591–612. The Combustion Institute, Pittsburgh, PA.

PUMIR, A. 1994 A numerical study of the mixing of a passive scalar in three dimensions in the presence of a mean gradient. *Phys. Fluids* **6**, 2118–2132.

PUMIR, A., SHRAIMAN, B. & SIGGIA, E. D. 1991 Exponential tails and random advection. *Phys. Rev. Lett.* **3**, 2838–2840.

ROGERS, M. M., MANSOUR, N. N. & REYNOLDS, W. C. 1989 An algebraic model for the turbulent flux of a passive scalar. *J. Fluid Mech.* **203**, 77–101.

ROGERS, M. M., MOIN, P. & REYNOLDS, W. C. 1986 The structure and modeling of the hydrodynamic and passive scalar fields in homogeneous turbulent shear flow. Department of Mechanical Engineering TF-25, Stanford University, Stanford, CA.

RUETSCH, G. R. & MAXEY, M. R. 1991 Small-scale features of vorticity and passive scalar fields in homogeneous-isotropic turbulence. *Phys. Fluids* A **3**, 1587–1597.

RUETSCH, G. R. & MAXEY, M. R. 1992 The evolution of small-scale structures in homogeneous-isotropic turbulence. *Phys. Fluids* A **4**, 2747–2760.

SANO, M., WU, X. Z. & LIBCHABER, A. 1989 Turbulence in helium gas free convection. *Phys. Rev.* A **40**, 6421–6430.

SHE, Z. S. 1990 Physical model of intermittency in turbulence: Near dissipation range non-Gaussian statistics. *Phys. Rev. Lett.* **66**, 600–603.

SHE, Z. S., JACKSON, E. & ORSZAG, S. A. 1991 Structure and dynamics of homogeneous turbulence: Models and simulations. *Proc. R. Soc. Lond. A* **434**, 101–124.

SHE, Z. S. & ORSZAG, S. A. 1991 Physical model of intermittency in turbulence: Inertial-range non-Gaussian statistics. *Phys. Rev. Lett.* **66**, 1701–1704.

SIGGIA, E. D. 1994 High Rayleigh number convection. *Ann. Rev. Fluid Mech.* **26**, 137–168.

SINAI, Y. G. & YAKHOT, V. 1989 Limiting probability distributions of a passive scalar in a random velocity field. *Phys. Rev. Lett.* **63**, 1962–1964.

SOLOMON, T. H. 1990 Transport and boundary layers in Rayleigh Bernard convection. PhD thesis, Department of Physics, University of Pennsylvania, Philadelphia.

SOLOMON, T. H. & GOLLUB, J. P. 1991 Thermal boundary layers and heat flux in turbulent convection: The role of recirculating flows. *Phys. Rev.* A **43**, 6683–6693.

TANAKA, M. & KIDA, S. 1993 Characterization of vortex tubes and sheets. *Phys. Fluids* A **5**, 2079–2082.

TAVOULARIS, S. & CORRSIN, S. 1981*a* Experiments in nearly homogenous turbulent shear flow with a uniform mean temperature gradient. Part 1. *J. Fluid Mech.* **104**, 311–347.

TAVOULARIS, S. & CORRSIN, S. 1981*b* Experiments in nearly homogenous turbulent shear flow with a uniform mean temperature gradient. Part 2. The fine structure. *J. Fluid Mech.* **104**, 349–367.

TENNEKES, H. & LUMLEY, J. L. 1972 *A First Course in Turbulence.* MIT Press.

THORODDSEN, S. T. & VAN ATTA, C. W. 1992 Exponential tails and skewness of density-gradient probability density functions in stably stratified turbulence. *J. Fluid Mech.* **244**, 547–566.

TONG, C. & WARHAFT, Z. 1994 On passive scalar derivative statistics in grid turbulence. *Phys. Fluids* **6**, 2165–2176.

TOOR, H. L. 1975 The non-premixed reaction: $A + B \rightarrow$ *Products.* In *Turbulence in Mixing Operations* (ed. R. S. Brodskey), pp. 123–166. Academic.

VAN ATTA, C. W. & ANTONIA, R. A. 1980 Reynolds number dependence of skewness and flatness factors of turbulent velocity derivatives. *Phys. Fluids* **23**, 252–257.

VAN ATTA, C. W. & CHEN, W. Y. 1970 Structure functions of turbulence in the atmospheric boundary layer over the ocean. *J. Fluid Mech.* **44**, 145–159.

VINCENT, A. & MENEGUZZI, M. 1991 The spatial structure and statistical properties of homogeneous turbulence. *J. Fluid Mech.* **225**, 1–20.

WARHAFT, Z. & LUMLEY, J. L. 1978 An experimental study of the decay of temperature fluctuations in grid-generated turbulence. *J. Fluid Mech.* **88**, 659–684.

YAKHOT, V. 1989 Probability distributions in high Rayleigh number Bernard convection. *Phys. Rev. Lett.* **63**, 1965–1967.

YAMAMOTO, K. & KAMBE, T. 1991 Gaussian and near exponential probability distributions of turbulence obtained from a numerical simulation. *Fluid Dyn. Res.* **8**, 65–72.

ZOCCHI, G., MOSES, E. & LIBCHABER, A. 1991 Coherent structures in turbulent convection: An experimental study. *Physica* A **166**, 387–407.